

1
2
3
4
5
6
7
8
9
10
11
12
13
14
15
16
17
18
19
20
21
22
23
24

PREPRINT SUBMITTED

This manuscript is a preprint uploaded to EarthArXiv, not yet peer-reviewed.

This preprint has been submitted for publication to Earth Surface Processes and Landforms on the 7th of March 2023. Authors encourage downloading the latest manuscript version from EarthArXiv, and welcome comments, feedback and discussions anytime. Please, feel free to get in contact with the first authors: denovan.chauveau@unive.it

25 **Unravelling the morphogenesis of coastal terraces at**
26 **Cape Laundi (Sumba Island, Indonesia): insights**
27 **from numerical models**

28
29
30 Denovan Chauveau^{a,b*}, Anne-Morwenn Pastier^c, Gino de Gelder^{d,e}, Laurent
31 Husson^d, Christine Authemayou^a, Kevin Pedoja^f, Sri Yudawati Cahyarini^e

32
33 ^a*Geo-Ocean UMR 6538, CNRS, Ifremer, Université de Bretagne Occidentale, F-29280 Plouzané,*
34 *France*

35 ^b*Dipartimento di Scienze Ambientali, Informatica e Statistica (DAIS), Ca' Foscari University of*
36 *Venice, Venice, Italy*

37 ^c*Helmholtz Centre Potsdam, German Research Centre for Geosciences (GFZ), Potsdam, Germany*

38 ^d*ISTerre, CNRS, IRD, UMR 5275, Université de Grenoble Alpes, Grenoble, France*

39 ^e*Res. Group of Paleoclimate & Paleoenvironment, Res. Centr. for Climate and Atmosphere, Res.*
40 *Org. of Earth Sciences and Maritime, National Research and Innovation Agency Republic of*
41 *Indonesia, Bandung, Indonesia*

42 ^f*Normandie Univ, Unicaen, Unirouen, M2C 1400, Caen, France*

43
44 *corresponding author : denovan.chauveau@unive.it /

45 chauveaudenovan@gmail.com

46
47 **Keywords:**

48 Numerical modeling, Geomorphology, Sea level, Marine Isotopic Stage, Coastal
49 terrace.

50 **Abstract**

51

52 The morphology of coastal sequences provides fundamental observations to
53 unravel past sea level (SL) variations. For that purpose, converting
54 morphometric observations into a SL datum requires understanding their
55 morphogenesis. The long-lasting sequence of coral reef terraces (CRTs) at Cape
56 Laundi (Sumba Island, Indonesia) could serve as a benchmark. Yet, it epitomizes
57 a pitfall that challenges the ultimate goal: the overall chronology of its
58 development remains poorly constrained. The polycyclic nature of the terraces,
59 involving marine erosion and reoccupation of old coral colonies by more recent
60 ones hinders any clear assignment of Marine Isotope Stages (MIS) to specific
61 terraces, in particular the reference datum corresponding to the last Interglacial
62 maximum (i.e., MIS 5e). Thus, to overcome these obstacles, we numerically
63 model the genesis of the sequence, testing a range of eustatic SL reconstructions
64 and uplift rates, as well as exploring the parameter space to address reef growth,
65 erosion, and sedimentation. A total of 625 model runs allowed us to improve the
66 morpho-chronological constraints of the coastal sequence and, more particularly,
67 to explain the morphogenesis of the several CRTs associated with MIS 5e. Our
68 results suggest that the lowermost main terrace was first constructed during the
69 marine transgression of MIS 5e and was later reshaped during the marine
70 regression of MIS 5e, as well as during the MIS 5c and MIS 5a highstands. Finally,
71 we discuss the general morphology of the sequence and the implications it may
72 have on SL reconstructions. At Cape Laundi, as elsewhere, we emphasize the
73 necessity to address the development of CRT sequences with a dynamic

74 approach, i.e., considering that a CRT is a landform built continuously throughout
75 the history of SL oscillations, and not simply during a singular SL maximum.

76

77 **1. Introduction**

78

79 Since the 19th century, sequences of coral reef terraces (CRTs) have been
80 described in the Caribbean province (e.g., Crosby, 1883; Peñalver et al., 2021),
81 in the Indo-Pacific province (e.g., Darwin, 1842; Pedoja et al., 2018), as well as
82 alongshore the Red Sea (e.g., Hume and Little, 1928; Obert et al., 2019).
83 Altogether, they provide a valuable database to infer sea level (SL) oscillations
84 during the Quaternary, both on a local/regional level (relative sea level; RSL)
85 and on a global level (eustatic sea level; ESL) (Pedoja et al., 2011, 2014; Rovere
86 et al., 2016a). Owing to their exceptional preservation and longevity, a few of
87 those are benchmarks to ESL studies (e.g., Barbados, Thompson and Goldstein,
88 2005; Huon Peninsula, de Gelder et al., 2022). Surprisingly, the long-lasting
89 emerged coastal sequence of Cape Laundi (Sumba Island, Indonesia), including
90 at least 18 successive CRTs and encompassing the last million years (e.g.,
91 Pirazzoli et al., 1991), is not included in these. The main reasons for this are the
92 diachronic nature and the particularly rounded morphology of the Cape Laundi
93 CRTs, challenging any reciprocal association of a terrace with a discrete SL
94 highstand. Indeed, various dating methods (U/Th; Electron Spin Resonance, ESR)
95 yield discrepant ages of the coral colonies within a unique CRT (e.g., Bard et al.,
96 1996). Conversely, previous dating also revealed similar ages on several distinct
97 CRTs. For example, ages of dated coral colonies ascribed to Marine Isotopic Stage

98 (MIS) 5e have been found on at least three different CRTs (Pirazzoli et al., 1991;
99 Bard et al., 1996). Such observations challenge the common bijective approach,
100 i.e., one-to-one pairing of a terrace and a SL highstand.

101

102 Here, in order to rehabilitate the Cape Laundi sequence for SL studies, we
103 explore the genetic links between ESL oscillations and the morphogenesis of this
104 sequence using a kinematic model based on reef morphology (Husson et al.,
105 2018; Pastier et al., 2019). We perform a parametric study using five ESL curves
106 (Waelbroeck et al., 2002; Bintanja et al., 2005; Rohling et al., 2009; Grant et
107 al., 2014; Spratt and Lisiecki, 2016) and a range of model parameters, including
108 uplift rate, basement slope, reef growth rate and marine erosion rate. From a
109 set of 625 simulations, based on nine morphological and chronological criteria,
110 we selected the best-fit to the Cape Laundi sequence for each ESL curve. This
111 further permits us to bracket the range of admissible parameters and to assign
112 ages for each CRT. We more specifically focus on the presence of several CRTs
113 associated with MIS 5e. We explain the overall morphology of the sequence and
114 in particular the roundness of distal edges of CRTs at Cape Laundi. Finally, our
115 study unravels the complex nature of CRTs, emphasizing the need to apply a
116 dynamic approach to understand their morphogenesis.

117

118 **2. Geomorphological setting**

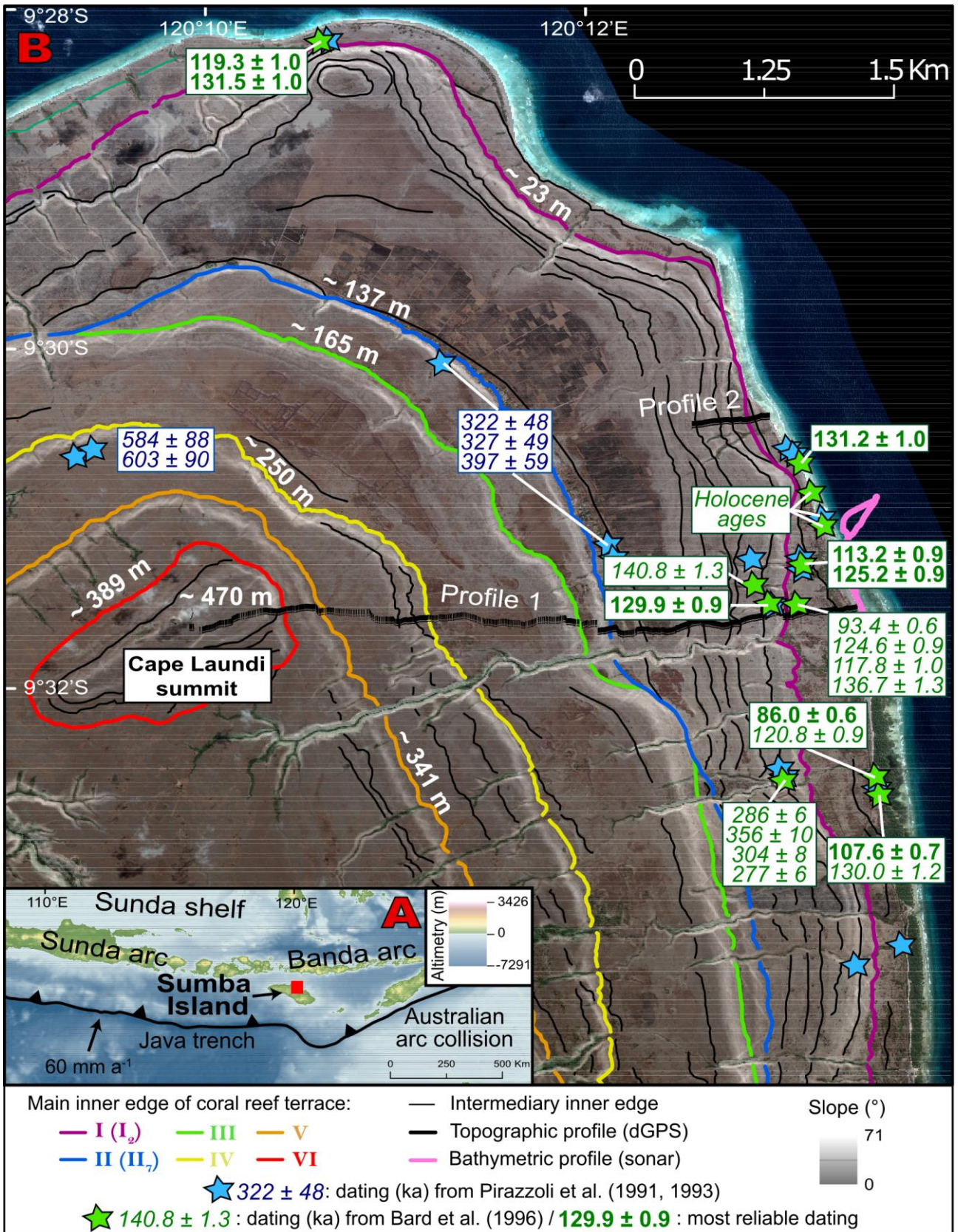
119

120 Sumba Island is located in the lesser Sunda-Banda arc (Fig. 1A), at the transition
121 from oceanic subduction in the West, along the Java trench, to the collision of

122 the Banda arc with the continental Indian-Australian plate in the East
123 (Hinschberger et al., 2005). Since the Late Miocene, the convergence between
124 Eurasia and the Indian-Australian plate shortened and uplifted the fore-arc
125 domain, where Sumba Island stands (e.g., Fortuin et al., 1997; Haig, 2012; Tate
126 et al., 2014; Husson et al., 2022). The Cretaceous to Oligocene crystalline
127 basement is almost entirely covered by Miocene and Pliocene deposits (Abdullah
128 et al., 2000), bordered by a ~350 km long emerged sequence of CRTs that record
129 the interplay between local SL variations and Quaternary uplift (e.g., Pirazzoli et
130 al., 1991; Bard et al., 1996; Nexer et al., 2015). The sequence spans
131 approximately two-thirds of the island shores. It is continuous all along the
132 northern shore of the island, only locally interrupted by large rivers (Fleury et
133 al., 2009; Nexer et al., 2015; Authemayou et al., 2018; Chauveau et al., 2021a).
134 To the south of the island, only a small CRTs sequence has been described
135 (Authemayou et al., 2022).

136

137 On the northeast coast of Sumba, live coral colonies are exclusively found on the
138 reef crest and on the fore reef slope (diving observation). The reef is comprised
139 of a few *Porites sp.* and branching corals (Hantoro, 1992). The back reef and
140 reef flat are characterized by a low density of live corals (i.e., coral cover <
141 10 %), mainly shallow species that are resistant to episodic emergence and/or
142 relatively high-water turbidity (e.g., *Goniastrea retiformis*, *Acropora digitifera*;
143 Bard et al., 1996) and by a coralgal environment.



144 **Fig. 1. A)** Altimetry map of Southeast Indonesia and location of Sumba Island
 145 and Cape Laundi (red square). Elevation data from the Shuttle Radar Topography
 146 Mission (SRTM), and bathymetry data from the General Bathymetric Chart of

147 Oceans (GEBCO), both at 90 m resolution. **B)** Slope map of Cape Laundi from
148 Pleiades satellite imagery. Contours delineate the inner edges of the CRTs, and
149 we indicate the location of previously dated samples (U/Th and Electron Spin
150 Resonance dating; Pirazzoli et al., 1991, 1993; Bard et al., 1996). Black and pink
151 curves indicate topographic (dGPS) and bathymetric (sonar) profile, respectively.

152

153 The Cape Laundi sequence in the central part of the northern shore reaches
154 ~470 m in elevation and has a staircase morphology with six main CRTs
155 separated by continuous high cliffs (> 10 m; Fig. 1B, Jouannic et al., 1988;
156 Pirazzoli et al., 1991). Most main CRT includes several intermediate CRTs, that
157 have a more diffuse morphology with surfaces and discontinuous cliffs weakly
158 sloping shoreward, and rounded distal parts (Hantoro et al., 1989; Pirazzoli et
159 al., 1993). The CRTs below CRT III are less wide and more seaward sloping than
160 those above (Fig. 1; e.g., Chauveau et al., 2021b).

161

162 Approximately fifty coral colonies from the surface of the four lowest main CRTs
163 have been dated (U/Th and ESR; Jouannic et al., 1988; Pirazzoli et al. 1991;
164 Bard et al., 1996). All ages were correlated to the ESL peaks of their associated
165 ESL highstands: MIS 15 (610 ± 10 ka), MIS 11 (390 ± 30 ka), MIS 9 ($325 \pm$
166 18.5 ka), MIS 7 (239.5 ± 8.5 ka), MIS 5e (122 ± 6 ka), MIS 5c (100 ± 5 ka),
167 MIS 5a (82 ± 3 ka), and MIS 1 (Pirazzoli et al., 1993; Bard et al., 1996). The
168 oldest dated CRT (V) has ESR ages of 584 ± 88 ka and 603 ± 90 ka and was
169 ascribed to MIS 15. The ages of the successive upper CRTs were extrapolated
170 assuming constant uplift rate (0.49 ± 0.01 mm a⁻¹), and thereafter associated

171 with ESL maximums up to ~ 1 Ma (MIS 29; Pirazzoli et al., 1993).
172
173 Several temporal discrepancies arose within the earliest dataset from a bijective
174 perspective (Pirazzoli et al., 1993). First, multiple U-series ages of corals were
175 found on the same CRT, and thus related to substages of the same MIS. For
176 example, ages of ~ 82 ka (MIS 5a) and ~ 138 ka (MIS 5e) are obtained from
177 coral colonies sampled on CRT I₁. Second, U-series ages related to MIS 5e were
178 found on corals from at least three distinct CRTs (138 ± 9 on CRT I₁; 114 ± 7 ,
179 119 ± 18 , 120 ± 8 , 124 ± 19 , 136 ± 8 , 142 ± 21 on CRT I₂; 148 ± 14 , $117 \pm$
180 18 , 133 ± 7 on CRT II₁; Pirazzoli et al., 1993). Finally, U-series ages and ESR
181 ages of corals from the same CRT do not always match with one another (e.g.,
182 148 ± 14 and 275 ± 41 on CRT II₁). TIMS (Thermal Ionisation Mass
183 Spectrometry) dating of corals (Bard et al., 1996) specified the diachronicity (i.e.,
184 ages associated to MIS 5a, 5c, and 5e on CRT I₁; MIS 5c and 5e ages on CRT
185 I₂). Previous authors (Jouannic et al., 1988; Pirazzoli et al., 1993; Bard et al.,
186 1996; Chauveau et al., 2021b) pointed at the diachronism on the lowermost CRT
187 I and inferred its composite nature, implying both constructive and erosive
188 reoccupation. Pirazzoli et al. (1993) suggested that local SL fluctuations
189 superimposed over a regular uplift rate of 0.5 mm a^{-1} must have caused
190 recurrent reoccupations of RSL over antecedent reefal constructions, capable of
191 reworking sediments, fostering abrasion or further developing bioconstructions
192 differing in age by as much as 100 ka on the same CRTs.

193

194 **3. Materials and Methods**

195

196 In this section, we explain, **1)** what CRTs sequence are, **2)** how we collected and
197 processed our field data, **3)** the numerical model used, and **4)** how we selected
198 the most robust previous dating.

199

200 **3.1. CRTs sequences**

201

202 CRTs are largely encountered in the tropical zones (Schwartz, 2006; Cabioch,
203 2011; Pedoja et al., 2011; 2014; Murray-Wallace and Woodroffe, 2014). When
204 ESL falls too rapidly and/or when the reef is uplifted by tectonic movements or
205 glacial isostatic adjustment (GIA), the reef (mainly fringing reefs) emerges and
206 fossilizes, forming a CRT. The joint effects of ESL oscillations, vertical land
207 movement and reef accretion can result in the generation of staircase CRT
208 sequences (Fig. 2; e.g., Chappell, 1974; Pirazzoli, 2005).

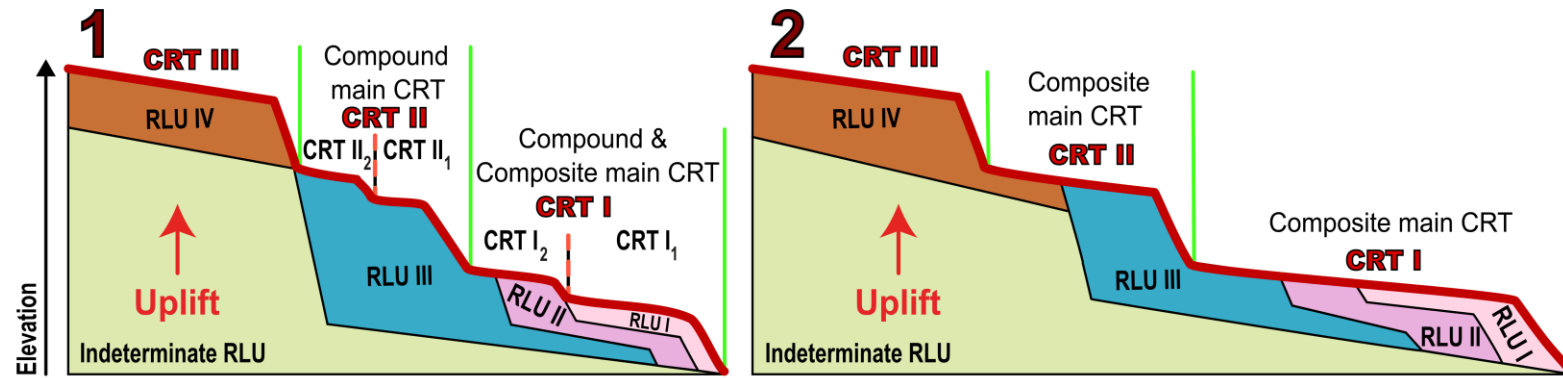
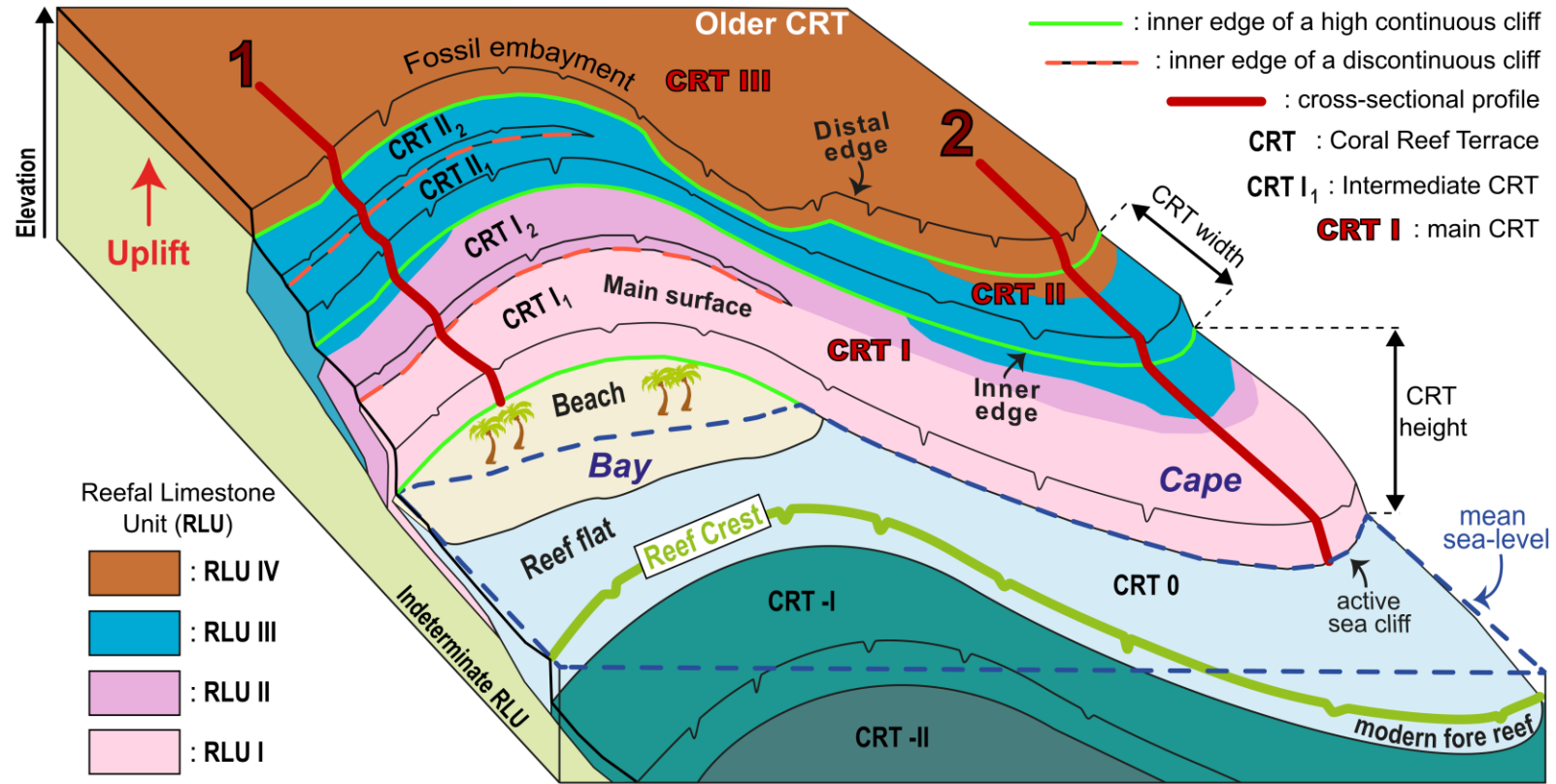
209

210 CRTs are expanses of reefal limestone with flat or slightly sloping surfaces,
211 limited seaward by a distal edge over a cliff of variable height (Fig. 2; e.g.,
212 Pirazzoli et al., 1991). The cliff separating successive CRTs is either an erosional
213 sea-cliff, a former fore-reef slope (sometimes very gentle as in Cape Laundi), or
214 a combination of both (e.g., Chappell, 1974). Landward, the inner edges of CRTs
215 are characterized by a break in slope, sometimes interpreted as a shoreline angle,
216 and occasionally associated with an erosional notch (e.g., Speed and Cheng,
217 2004; see Figure 3 in Pedoja et al., 2018). In general, the elevation of a CRT

218 taken as a reference point for RSL calculations corresponds to its average
219 elevation, its inner edge, or, if present, to the elevation of the highest *in situ*
220 corals that are usually found on the paleo reef crest (Rovere et al., 2016b).
221 However, the difference in elevation between the inner and distal edges of most
222 CRTs can be -in some cases, such as Cape Laundi- too important to consider that
223 the average elevation of the CRT is representative of the ancient reef that built
224 it or that the distal edge corresponds to the paleo reef crest. Furthermore, the
225 distal edge of CRTs is affected by higher continental denudation rates than the
226 other proximal parts (Chauveau et al., 2021b). In addition, we consider here
227 that the width and height of a CRT correspond respectively to the horizontal
228 distance and elevation difference between the two adjacent inner edges (Fig. 2).

229

230 The morphology and stratigraphy of CRTs result from interactions between reef
231 accretion (bioconstruction and sedimentation), marine erosion, RSL change
232 (local SL variations and vertical land motion) and geometry of the basement
233 (e.g., Pirazzoli, 2005; Cabioch, 2011; Husson et al., 2018; Pedoja et al., 2018;
234 Pastier et al., 2019). These numerous interactions account for a wide spectrum
235 of CRT morphologies (Fig. 2). At Cape Laundi, one CRT with a continuous high
236 fossil sea cliff (> 10 m; see CRT I in Figure 2) can include numerous secondary
237 or intermediate CRTs (CRTs I₁ and I₂ in Figure 2) with or without low (< 10 m),
238 eroded, fossil sea cliffs and multiple associated reefal limestone units (RLUs;
239 Hantoro et al., 1989; Pirazzoli et al., 1993). We refer to these landforms as main
240 CRTs (Fig. 2; e.g., Chauveau et al., 2021b).



242 **Fig. 2.** Sketch of a sequence of coral reef terraces (CRTs), modified from Pedoja et al. (2018), highlighting a high
243 variability of sequence morphology that can occur for a uniform uplift. The inner edges of the main CRT I and CRT II
244 are continuous from the bay to the cape, the inner edges of the CRT I₁ and CRT II₁ are not. Depending on the location
245 along the coast (Bay or Cape), the main CRT II is either compound, i.e., consisting of two CRTs (i.e., CRT II₁ et II₂)
246 but a single reefal limestone unit (i.e., RLU III; Profile 1), or composite, i.e., consisting of a single CRT (i.e., CRT II)
247 but including several RLUs (i.e., RLU III and IV; Profile 2). The RLUs can be associated with different MIS. The
248 stratigraphy and the thickness, and therefore the depth, of the RLUs are approximations.

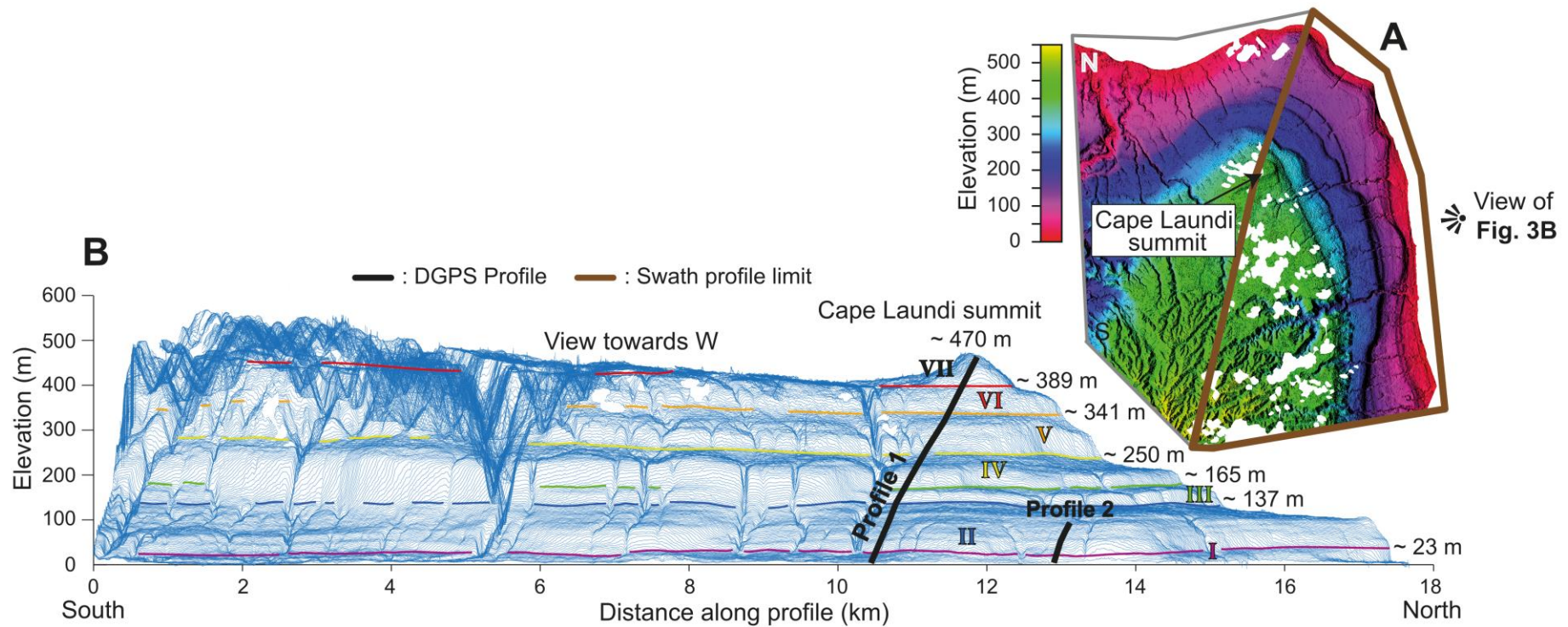
249 Theoretically, when these main CRTs include several intermediate CRTs but
250 are formed by only one RLU (main CRT II on the Profile 1 in Figure 2), we
251 call them compound main CRTs (see Figure 2 in Pedoja et al., 2014). On the
252 contrary, when a CRT does not include intermediate CRTs but is formed by
253 several RLUs (see main CRTs I and II on the Profile 2 in Figure 2), associated
254 to distinct RSL highstands, we call it composite CRT (see Figure 3 in Pedoja
255 et al., 2018). Finally, when a main CRT includes several intermediate CRTs
256 and is formed by several RLUs (main CRT I on the Profile 1 in Figure 2), we
257 call it compound and composite main CRT.

258

259 **3.2. Onshore and offshore morphometry**

260

261 We mapped the inner edges of CRTs at Cape Laundi using a 2 m resolution
262 Digital Elevation Model (DEM) produced from stereoscopic satellite images
263 (Pleaidés, CNES) with MicMac freeware (e.g., Rupnik et al., 2016). To assess
264 the lateral continuity of the CRTs sequence, we used stacked swath profiles
265 (Armijo et al., 2015; Fernández-Blanco et al., 2019), constructed using
266 many parallel swath profiles (Fig. 3) to derive a 2.5-D view of the landscape.
267 On swath profiles, CRTs are revealed by areas with clusters of overprinted
268 topographic profiles that are indicative of the flatness of the topography.



269 **Fig. 3. A)** Hillshade map of the Digital Elevation Model (~2 m in resolution) based on Pleiades satellite imagery and
 270 the point of view for the stacked swath profiles. The white spots inside the hillshade correspond to the clouds in the
 271 Pleiades images. **B)** Stacked swath profiles (600 profiles evenly distributed over the area shown in A, exaggeration
 272 x6) and inner edges of the main CRTs at Cape Laundi. Most main CRTs show lateral morphological variability in the
 273 number of intermediate terraces, while the elevation of their inner edge is very stable, highlighting a uniform uplift
 274 rate along the coast.

275 We acquired topographic and bathymetric profiles, using a real kinematic
276 differential global positioning system (RTK dGPS) onshore (elevations are
277 converted to orthometric heights, following Boulton and Stokes, 2018), and
278 a Humminbird 700 series sonar offshore (Figs. 1B; 3B). Onshore, our
279 profiles are parallel to the profile investigated by Pirazzoli et al. (1993) and
280 runs perpendicular to the inner edges of the successive CRTs. Profile 1
281 crosses the whole sequence while Profile 2 is designed to focus on the lowest
282 CRTs (Figs. 1B; 3B). Here, taking advantage of the high-resolution
283 topographic data (Pleiades imagery, DEM and dGPS), we revised the
284 nomenclature of CRTs (Table 1). We assigned an elevation uncertainty to all
285 field measurements as a function of the observed roughness of the landform
286 (± 0.5 m below 250 m; ± 1.5 m above 250 m, as defined in Chauveau et
287 al., 2021b).

Nomenclature of the CRTs		MIS associated with CRTs		Elevation of CRTs			Width of CRTs	
Pirazzoli et al. (1991, 1993)	This study	Pirazzoli et al. (1991, 1993)	This study	Pirazzoli et al. (1991, 1993) (Elevation of former reef crest; m)	This study (Elevation of inner edge; dGPS; m)	Best-fit simulation (Elevation of inner edge; ± 1 m)	This study (dGPS ; ± 1 m)	Best-fit simulation (± 1 m)
CRT O1	CRT O	MIS 1	MIS 1	1.1 ± 0.5	0 ± 0.5	0	288	359
CRT I1	CRT I1	MIS 5	MIS 1; 5a; 5c	3.5 ± 0.5	6.4 ± 0.5	12	182	313
CRT I2	CRT I2	MIS 5	MIS 5c; 5e	19 ± 1	23.2 ± 0.5	19	484	242
CRT II1	CRT II0	MIS ?	MIS 5e		42.4 ± 0.5			
CRT II2	CRT II1	MIS 5; 7	MIS 5e	50 ± 5	57.1 ± 0.5	63	251	399
CRT II3	CRT II2	MIS 5; 7; 9	MIS 5e; 7a; 7c	62 ± 5	76.0 ± 0.5	78	218	261
CRT II4	CRT II3	MIS 7; 9	MIS 7c; 7e		79.9 ± 0.5	86	73	207
	CRT II4				95.0 ± 0.5	100	312	141
CRT II5	CRT II5	MIS 9	MIS 9a; 9c/e		105.4 ± 0.5	101	135	259
	CRT II6				119.3 ± 0.5	123	367	190
CRT III1	CRT II7	MIS 9	MIS 9c/e	145 ± 10	136.6 ± 0.5	137	312	305
CRT III2	CRT III	MIS 11	MIS 11		165.4 ± 0.5	163	293	457
CRT III3	CRT IV	MIS 13	MIS 13		250.5 ± 1.5	248	1514	1426
CRT IV1; IV2	CRT V	MIS 15; 17	MIS 15; 17	275 ± 10	341.0 ± 1.5	324	1086	1434
CRT IV3; V0; V1; V2	CRT VI	MIS 19; 21; 23	MIS 19; 21; 23		389.3 ± 1.5	413	279	1567
CRT VI1; VI2	CRT VII	MIS 25; 27; 29	MIS 25; 27; 29		470 ± 1.5	470		

289 **Table 1.** Nomenclature (from Pirazzoli et al., 1991, 1993, and revised in this study), associated MIS (i.e., Marine
290 Isotopic Stage), elevation, width of CRTs (i.e., Coral Reef Terraces) from previous studies (Pirazzoli et al., 1991,
291 1993), dGPS (i.e., differential Global Positioning System) field measurements and our best-fit simulation (obtained
292 with the sea level reconstruction of Bintanja et al., 2005).

3.3. Modeling CRTs sequences

293

294

295 Since the earliest work of Chappell (1980), many other numerical models
296 of reef growth have been developed (e.g., Bosscher and Schlager, 1992;
297 Turcotte and Bernthal, 1984; Webster et al., 2007; Koelling et al., 2009;
298 Toomey et al., 2013). Here, we use a kinematic profile evolution model,
299 combining the effects of reef growth, marine erosion, and deposition of
300 subsequent clastic sediments (Husson et al., 2018; Pastier et al., 2019).

301 The variation of the elevation profile through time ($\frac{ds}{dt}$) is defined by:

302

$$303 \quad \frac{ds}{dt} = \frac{dG}{dt} + \frac{dE}{dt} + \frac{dS}{dt} + U \quad (1)$$

304

305 Where $\frac{dG}{dt}$, $\frac{dE}{dt}$ and $\frac{dS}{dt}$ respectively represent the contribution of reef growth,
306 marine erosion, and clastics deposition. U is the vertical land motion rate.
307 Reef growth is defined by a maximum potential reef growth rate G_{max} ,
308 modulated by a vertical factor γ and a horizontal factor ζ :

309

$$310 \quad \frac{dG}{dt} = G_{max} \times \gamma \times \zeta \quad (2)$$

311

312 The vertical factor γ accounts for decreasing coral growth rate with
313 increasing water height due to light attenuation. It is controlled by the local
314 water height along the profile, $h(s)$, and a maximum water height for
315 significant coral growth, h_{max} :

316

$$317 \quad \gamma = \frac{1}{2} \left(1 + \cos \frac{\pi h(s)}{h_{max}} \right) \quad (3)$$

318

319 The horizontal factor accounts for decreasing coral growth from the reef
320 crest shoreward. It is controlled by the distance to the location of the open
321 water, x_{ow} , defined by the first occurrence of the optimum water height for
322 reef growth, h_{ow} in the bathymetry, and a distance δ defining the rate of
323 coral growth decrease along the profile:

324

$$325 \quad \zeta = \frac{1}{2} \left(1 + \tanh \frac{x_{ow} - x}{\delta} \right) \quad (4)$$

326

327 Marine erosion is based on the model of Anderson et al. (1999), where an
328 initial erosional potential E_0 first erodes the sea-bed at each location along
329 the profile depending on the local water height, h , the water height for wave
330 base erosion, h_{wb} , and a coefficient for sea bed erodibility K , such as:

331

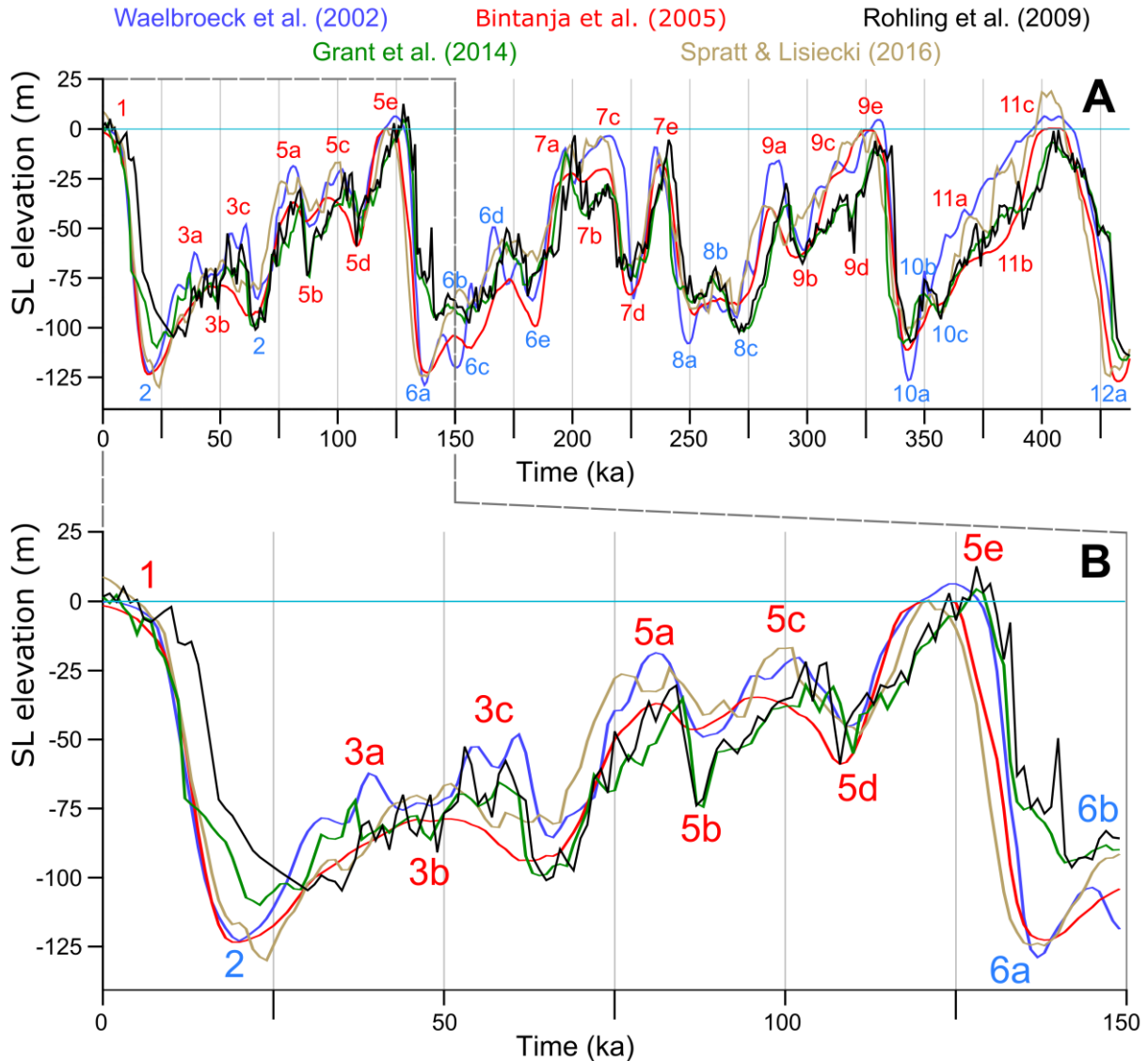
$$332 \quad \frac{dE}{dt} = K \frac{dE_0}{dt} \exp \left(- \frac{h}{h_{wb}} \right) \quad (5)$$

333

334 Clastic deposition occurs horizontally in lagoons and along a repose angle
335 of 10 % at the foot of the forereef slope. The initial profile is imposed as a
336 linear slope (α). The temporal and spatial resolution are respectively 1 ka
337 and 1 m (see Pastier et al. (2019) for more details).

338

339 Local SL variations are equally crucial. Yet, uncertainties in Quaternary ESL
340 variations are high (Fig. 4; e.g., Caputo, 2007) and the choice of a specific
341 ESL or RSL curve may greatly affect the model outcome (e.g., De Gelder et
342 al., 2020). We chose five reconstructed ESL curves, i.e., Waelbroeck et al.
343 (2002); Bintanja et al. (2005); Rohling et al. (2009); Grant et al. (2014);
344 Spratt and Lisiecki (2016). The resulting best-fit simulations are named
345 W02, B05, R09, G14, and S16 (Fig. 4). We note that ideally GIA-corrected
346 RSL curves should be used that are adjusted to local effects at Cape Laundi,
347 but such curves are currently not available, and given Sumba's far-field
348 location, differences would only be on the order of a few meters. In the
349 following we use ESL when discussing the general characteristics of SL
350 during the different MIS stages and the SL reconstructions used, and RSL
351 when discussing the relative changes of SL with respect to the land/reef at
352 Cape Laundi.



353 **Fig. 4.** Eustatic sea level (SL) curves used in this study from **A)** 435 ka and
 354 **B)** 150 ka to today. MIS nomenclature (numbers and letters) from Railsback
 355 et al. (2015). SL curves are at low (Waelbroeck et al., 2002; Bintanja et al.,
 356 2005), intermediate (Grant et al., 2014; Spratt and Lisiecki 2016), and high
 357 (Rohling et al., 2009) frequencies. SL rate peaks of the different curves are
 358 generally coeval; however, they differ in their frequencies and amplitudes.
 359 During MIS 5e, SL curves can show two episodes of fast SL change during
 360 the prior transgression (Rohling et al., 2009; Grant et al., 2014) and several
 361 highstand peaks (Rohling et al., 2009).

362 The reconstruction of Waelbroeck et al. (2002) is based on oxygen isotopic
363 ratios of benthic foraminifera from the North Atlantic and Equatorial Pacific
364 Ocean over the four last glacial-interglacial cycles, calibrated with the
365 elevation of coral samples corrected from vertical deformation. Bintanja et
366 al. (2005) used numerical modeling to reconstruct ESL variations and
367 continental ice volume over 1 Ma from a continuous global compilation of
368 benthic oxygen isotope data. Rohling et al. (2009) and Grant et al. (2014)
369 used the oxygen isotopic ratios of planktonic foraminifera from the central
370 Red Sea over 500 ka, while inferring those local variations are roughly
371 representative of ESL. Last, the meta-analysis of Spratt and Lisiecki (2016)
372 is based on a principal component analysis of earlier compilations
373 (Waelbroeck et al., 2002; Bintanja et al., 2005; Sosdian and Rosenthal,
374 2009; Rohling et al., 2009; Elderfield et al., 2012; Rohling et al., 2014;
375 Shakun et al., 2015), up to 800 ka. As a consequence of the different
376 reconstruction methods, these ESL curves span a range of temporal lengths
377 and resolutions.

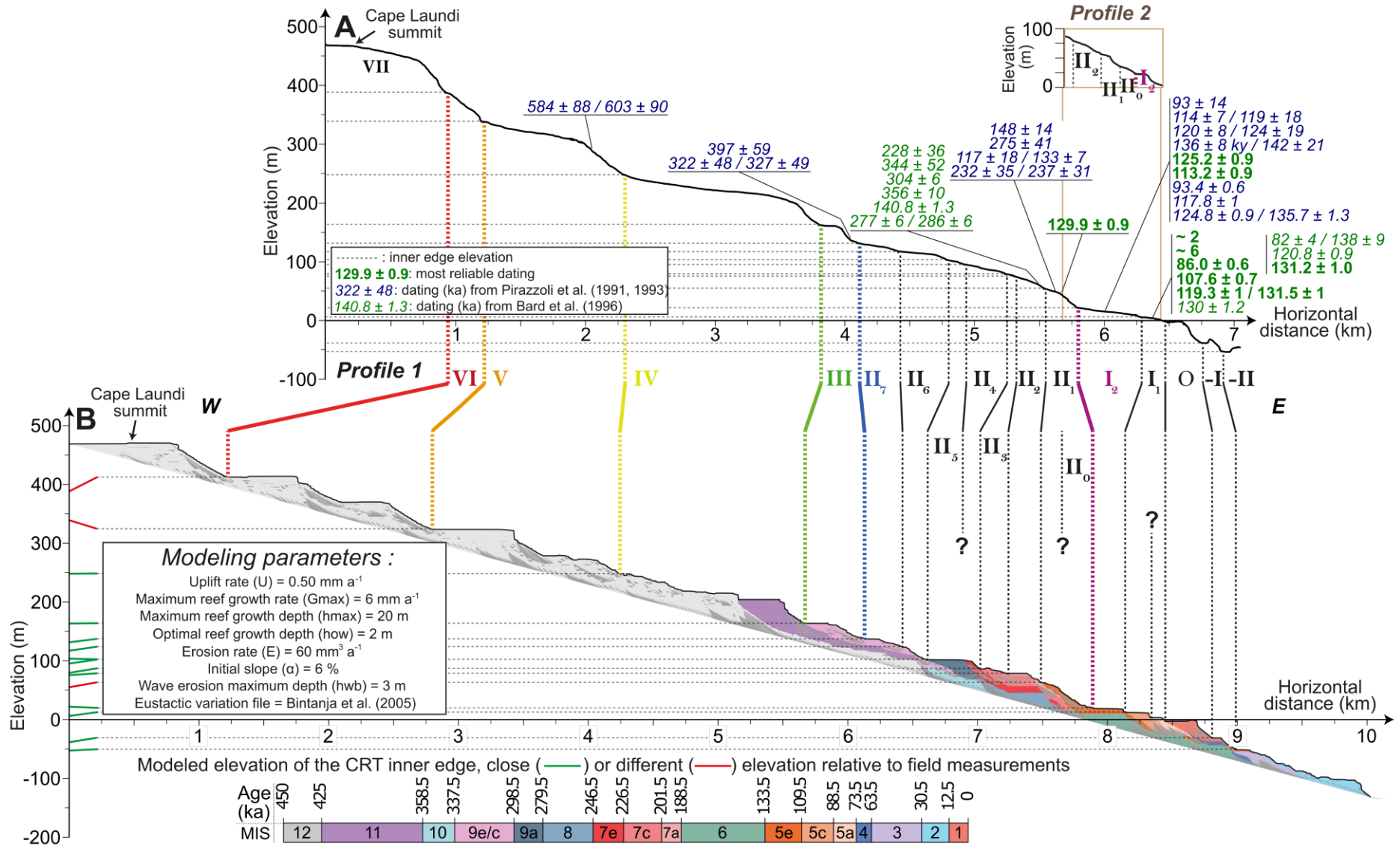
378

379 We modeled the Cape Laundi sequence with ranges of uplift rates (U : 0.42-
380 0.52 mm a⁻¹, every 0.02 mm a⁻¹), maximum reef growth rates (G_{\max} : 4-16
381 mm a⁻¹, every 2 mm a⁻¹), erosion rates (E : 20-60 mm³ a⁻¹, every 10 mm³
382 a⁻¹), and initial basement slope (α : 5-7 %, every 1 %). The choices of
383 ranges are either restricted because they are justified by previous studies
384 (i.e., U and α ; Pirazzoli et al., 1993; Nexer et al., 2015), or they are
385 somewhat restricted by our field observations (i.e., G_{\max} ; the coral cover of

386 the modern Cape Laundi reef being estimated at 50 %), or they cover a
387 large range because they are not constrained, either by previous studies or
388 by field observations (i.e., E). The maximum and optimal reef growth depths
389 (h_{ow}) and the maximum depth of wave erosion (h_{wb}) are set to 20 m
390 (Bosscher and Schlager, 1992), 2 m and 3 m, respectively, based on our
391 field observations. Each of the 625 simulations is compared to the
392 morphometric data (dGPS and sonar), and radiometric ages (i.e., U/Th- and
393 ESR-dating) for the Cape Laundi sequence (Fig. 5A; Pirazzoli et al., 1993;
394 Bard et al., 1996).

395

396 We scored each numerical simulation based on the outcrop of reef
397 construction in agreement with robust ages and 9 morphological criteria in
398 order of importance: the morphology (i.e., overall shape of the CRT and
399 elevation of surrounding inner edges) of **1)** CRT II₁, **2)** CRT I₂, **3)** CRT II,
400 **4)** modern reef, **5)** CRT III, **6)** CRT IV, **7)** occurrence of two submerged
401 CRTs, **8)** occurrence of a submerged barrier reef, **9)** inner edge of CRT II₀
402 (elevation of ~40 m and only observable on profile 2; Fig. 5A).



404 **Fig. 5. A)** Morphometric profiles (dGPS and sonar) at Cape Laundi, showing the location and ages of U/Th and
405 Electron spin resonance (ESR) samples (Pirazzoli et al., 1991, 1993; Bard et al., 1996). **B)** Best-fit numerical
406 simulation (obtained with B05; U (uplift rate): 0.50 mm a^{-1} ; G_{max} (maximum reef growth rate): 6 mm a^{-1} ; E (erosion
407 rate): $60 \text{ mm}^3 \text{ a}^{-1}$; α (initial slope): 6 %). The red and green lines (near the y-axis) show the modeled elevations of
408 the CRT inner edges, close to or different from field measurements, respectively. Two inner edges measured in the
409 field (i.e., associated with CRT II₄, and II₀) do not correlate with any of the simulated inner edges (they are marked
410 with a "?"). Conversely, one simulated inner edge (in the middle of simulated CRT I₁) does not correlate with any
411 field measurements (also marked with a "?"). The full description of the simulated CRT sequence is in section 4.1..

3.4. Selection of robust dating

412
413
414 We selected U-series ages from previous studies (Pirazzoli et al., 1991, 1993;
415 Bard et al., 1996), following Broecker and Thurber (1965) and Obert et al.
416 (2016), requiring **1)** lack of recrystallisation of the primary aragonite (less
417 than 2 % calcite), **2)** ^{238}U concentration in the range of modern coral species
418 (2.75 ± 0.55 ppm; e.g., Robinson et al., 2003; Lazar et al., 2004; Scholz et
419 al., 2004), **3)** low values of ^{232}Th (< 0.0004 ppm) and high values of
420 $^{230}\text{Th}/^{232}\text{Th}$ (> 200 ; e.g., Scholz et al., 2004), and **4)** $^{234}\text{U}/^{238}\text{U}$ values which,
421 combined with apparent $^{230}\text{Th}/^{234}\text{U}$ ages, give back-calculated initial
422 $^{234}\text{U}/^{238}\text{U}$ values that are in the range of modern seawater ($\delta^{234}\text{U} = 146.6$
423 ± 1.4 ‰; Delanghe et al., 2002). We retained 8 samples out of 50
424 Pleistocene dated samples. These eight ages (samples SBA 9; 10; 12; 14;
425 15; 16; 17; 22 in Bard et al., 1996 and in bold in Figures 1 and 5A) are
426 therefore the most reliable ages obtained at Cape Laundi.

4. Results

427
428
429
430 Here we detail the results from the model used (i.e., Pastier et al., 2019),
431 **1)** showing the parameter ranges obtained for the best-fit simulations (i.e.,
432 B05, W02, R09, G14, S16), then **2)** comparing the best-fit simulation
433 obtained (i.e., B05) with the field measurements data and the chronological
434 constraints for the whole sequence, and **3)** comparing the other best-fit
435 simulations (i.e., W02, R09, G14, S16) with the same data but only for the

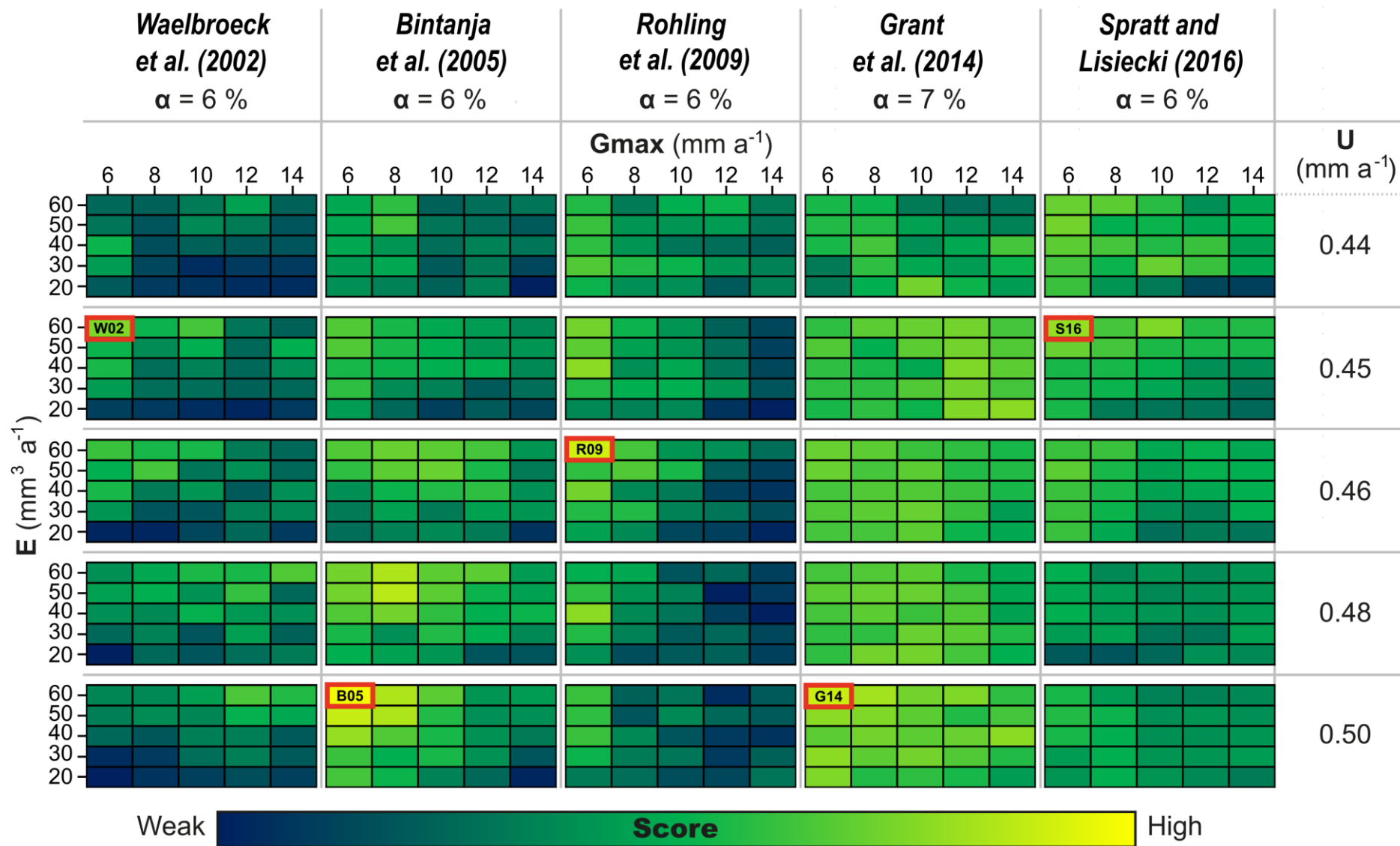
436 lower part of the Cape Laundi sequence.

437

438 **4.1. CRTs sequence at Cape Laundi**

439

440 Resulting scores are given in Figure 6. We identified clusters of good scores
441 and selected the best-fit simulation for each ESL curve (Fig. 6). High score
442 simulations are obtained with **1)** uplift rates (U) ranging between 0.45 mm a^{-1}
443 a^{-1} (W02 and S16), 0.46 mm a^{-1} (R09), and 0.50 mm a^{-1} (B05 and G14), in
444 line with previous studies (Pirazzoli et al., 1993; Nexer et al., 2015), **2)** a
445 maximum reef growth rate (G_{max}) of 6 mm a^{-1} , in agreement with
446 observations of the modern reef coral cover (section 2.), corresponding to
447 an effective reef growth rate of about 4 mm a^{-1} (section 3.3.), **3)** an erosion
448 rate (E) of $60 \text{ mm}^3 \text{ a}^{-1}$, and **4)** an initial slope (α) of 6-7 % (Fig. 6).
449 Therefore, despite the differences between the ESL reconstructions used
450 (Fig. 4), the best-fit simulations selected constrain the sequence
451 morphogenesis parameters over similar parametric ranges.



453 **Fig. 6.** Parametric study, simulations scores for 5 eustatic sea level (ESL) curves (columns), uplift rates (U; rows),
454 maximum reef growth rates (G_{\max} ; x axis) and erosion rates (E; y axis). The color of each "small box" represents
455 the score of the simulation for a given parametrization based on the chrono-morphological criteria defined in section
456 3.3. Each "medium box" shows simulation scores for the range of maximum reef growth rate, G_{\max} , and the range
457 of erosional potential E_0 (see section 3.3.). Each line of "medium boxes" shows the variability along the range of
458 uplift rates. Each column of "medium boxes" shows the variability among ESL reconstructions. The best-fitting initial
459 slope (α) is indicated for each SL reconstruction. The best-fit simulations are surrounded by a red square with the
460 names designated in section 3.3. (i.e., W02, B05, R09, G14, and S16).

4.2. The best-fit simulation for Cape Laundi

461
462
463
464
465
466
467
468
469
470
471
472
473
474
475
476
477
478
479
480
481
482
483
484

The highest score simulation (Fig. 6) is obtained with the ESL curve of Bintanja et al. (2005). It most accurately predicts the morphology of the lower CRTs of the sequence (i.e., the CRTs below CRT III) and to the roundness of the distal edges of CRTs (Fig. 5A). Thus, to improve the interpretation of the CRTs sequence, we studied **1)** the spatial differences between B05 (U: 0.50 mm a⁻¹; G_{max}: 6 mm a⁻¹; E: 60 mm³ a⁻¹; α: 6 %) and our field measurements, and **2)** the temporal differences between the chronological constraints derived from this simulation and existing dating (Table 1).

CRT I₁ has a measured width of 180 m and an inner edge raised at 6.4 ± 0.5 m (Fig. 5A) whereas its simulated width amounts to 312 m and its inner edge elevation lies at 12 m (Fig. 5B). If we consider only robust datings (see section 3.4.), CRT I₁ ages range from 2 ka to 131 ka. B05 also suggests that this CRT is composite, but with consistent ages of MIS 5c and 5a (Fig. 5B). CRT I₂ is 484 m wide, and its inner edge is found at 23 m (Fig. 5A). The simulation suggests a width half that of the measured one and an elevation of the inner edge of 19 m (Fig. 5B). On this CRT, coral colonies have been dated from 93 ± 14 ka to 142 ± 21 ka by Pirazzoli et al. (1993) and from 93.4 ± 0.6 ka to 135.7 ± 1.3 ka by Bard et al. (1996). The simulation proposes an age correlated with MIS 5e (109.5 to 133.5 ka; Fig. 5B).

The simulated CRT II₁ has a maximum elevation of 63 m and a width of ~400

485 m; field measurements yield 57 m and 215 m respectively (Table 1; Fig. 5).
486 Pirazzoli et al. (1993) obtained ages ranging from 117 ± 18 ka to 275 ± 41 ka
487 from coral colonies sampled on the CRT surface. The only robust age of this CRT
488 is 129.9 ± 0.9 ka (Bard et al., 1996). The best-fit simulation suggests a reef
489 construction during MIS 5e (Fig. 5B). CRT II₂ has a width of 218 m and a
490 maximum elevation of 76 m (Fig. 5A). The simulation width and elevation of this
491 CRT are 261 m and 78 m, respectively (Table 1). The coral colonies dated on this
492 CRT show very heterogeneous ages, ranging from 140.8 ± 1.3 ka to 356 ± 10
493 ka (Fig. 5A), leading to a possible correlation of the CRT with MIS 6 as well as
494 with MIS 11. For CRT II₂, the simulation suggests ages between 118.5 and 226.5
495 ka, which suggests a correlation with MIS 7c and MIS 7a. In the field, CRT II₃
496 has a narrow width of 73 m and a maximum elevation of 80 m (Table 1). In the
497 simulation, it reaches a width of 207 m and an elevation of 86 m. The simulated
498 surface of CRT II₃ does not match the overall shape observed in the field (Fig.
499 5). In addition, there are no chrono-stratigraphic constraints for the RLUs
500 forming CRT II₃ (Fig. 5A). Simulations suggests a possible correlation with MIS
501 7c (Fig. 5B). CRT II₄ is 312 m wide and has a maximum elevation of 95 m in the
502 field. The simulation does not suggest any terrace (Fig. 5B). Again, there is no
503 age chrono-stratigraphic constraints for RLUs composing this CRT. However, the
504 simulation gives a correlation with MIS 7e (Fig. 5B). In the field and in the
505 simulation, CRT II₅ has a width of 135 m and 259 m and an inner edge elevation
506 of 105.4 ± 0.5 m and 101 m, respectively. For the RLUs forming CRT II₅, the
507 simulation suggests an age between 279.5 and 298.5 ka (i.e., corresponding to
508 MIS 9a; Fig. 5B).

509

510 The simulation highlights an elevation and width of 123 m and 190 m for CRT
511 II₆, where the field measurements show 119 m and 367 m, respectively. For this
512 CRT, the simulation suggests an age ranging between 298.5 and 337.5 ka
513 associated to MIS 9e/c. CRT II₇ reaches a maximum elevation of 137 m, both by
514 the field measurements and the simulation (Table 1; Fig. 5). The width of this
515 CRT is measured at 312 m and 305 m with the dGPS and the simulation,
516 respectively. The simulation also suggests an age correlated to MIS 9c/a for this
517 CRT. CRT III has a measured width of 293 m (457 m with the simulation) and
518 an inner edge elevation found at 165 m (163 m with the simulation). Three ages
519 were previously obtained for this CRT: 322 ± 48 , 327 ± 49 and 397 ± 59 ka (Fig.
520 5A; Pirazzoli et al., 1993). The simulation suggests a correlation with MIS 9e/c.
521 Thus, the results of the present study highlight the possible formation of three
522 distinct CRTs (II₆, II₇ and III) during MIS 9e/c.

523

524 The stacked swath profiles (Fig. 3) reveal the lateral morphological variability of
525 the upper CRTs: some intermediate CRTs are not present laterally at Cape Laundi.
526 Moreover, besides two ages with large uncertainties (i.e., 584 ± 88 and $603 \pm$
527 90 ka on the distal edge of CRT V; Pirazzoli et al., 1993) no age constraint exist
528 on CRT IV, which does not help interpreting our simulations. Nevertheless, the
529 simulation successfully reprocesses the morphometric observations related to
530 CRT IV (CRT width and inner edge elevation; Table 1). More precisely, the
531 measured length and elevation are 1514 m and 251 m, where the simulation
532 predicts 1426 and 248 m. The distal edge of this CRT has a simulated age

533 ranging from 358.5 to 425 ka. We suggest a correlation with MIS 11 in
534 conformity with previous studies (Nexer et al., 2015). For the upper part of the
535 Cape Laundi sequence, the discrepancy between the simulation and field
536 observations become more important. For example, the inner edges of CRTs V
537 and VI are measured in the field at 341 and 389 m, where the simulation yielded
538 324 and 413 m. The same applies to the widths of these two CRTs, which are
539 measured at 1086 m and 279 m, whereas the simulation gives widths of 1434
540 and 1567 m. Concerning the age estimations of these CRTs, our results are in
541 agreement with previous studies (i.e., correlation from MIS 15 to MIS 23; Fig.
542 5; Pirazzoli et al., 1993). Finally, concerning the highest CRT of Cape Laundi (VII),
543 our simulation suggests an elevation of 470 m (such as our field measurements;
544 Fig. 5) and an age of formation at MIS 29, 27 and 25, in agreement with earlier
545 studies (Pirazzoli et al., 1993).

546

547 **4.3. Comparison of the modeled lower part of the sequence** 548 **obtained with the different simulations**

549

550 Here the results of the simulations (other than B05) are presented for the lower
551 part of the sequence (i.e., main CRT II and I; the full best-fit simulations are
552 available in the supplementary data, as well as the animations for each best-fit
553 simulation).

554

555 The simulated morphology of the main CRT II with W02 (U : 0.45 mm a⁻¹; G_{\max} :
556 6 mm a⁻¹; E : 60 mm³ a⁻¹; α : 6 %; Fig. 7B) is relatively consistent with our

557 measurements (Fig. 5A). In addition, this simulation predicts a CRT that is only
558 present on dGPS profile 2 (CRT II₀; Figs. 4A; 7A). However, no RLU related to
559 MIS 5e is simulated on CRT I₁ and I₂, which is at odds with previous work
560 (Pirazzoli et al., 1993; Bard et al., 1996). Finally, W02 suggests the initiation of
561 a drowned barrier reef as observed offshore Cape Laundi (Figs. 5A; 7A;
562 Chauveau et al., 2021b).

563

564 R09 (U: 0.46 mm a⁻¹; G_{max}: 6 mm a⁻¹; E: 60 mm³ a⁻¹; α: 6 %) also show this
565 submerged barrier reef (Fig. 7B). This simulation predicts a 136 m wide Holocene
566 CRT raised at 3.5 m above mean SL. This result can be explained by the high
567 frequency of this ESL curve (Fig. 4). Then, the simulated main CRT I has a
568 morphology close to the observed one. However, this simulation shows mainly
569 outcropping RLU associated with MIS 5c (Fig. 7B). Some outcrops of RLUs
570 related to MIS 5a and 5e are obtained on CRT I₁ and at inner edge of CRT I₂,
571 respectively (Fig. 7B). As observed in the field, the simulated morphology of the
572 intermediate CRTs of the main CRT II is characterized by weakly sloping distal
573 parts (Fig. 7B).

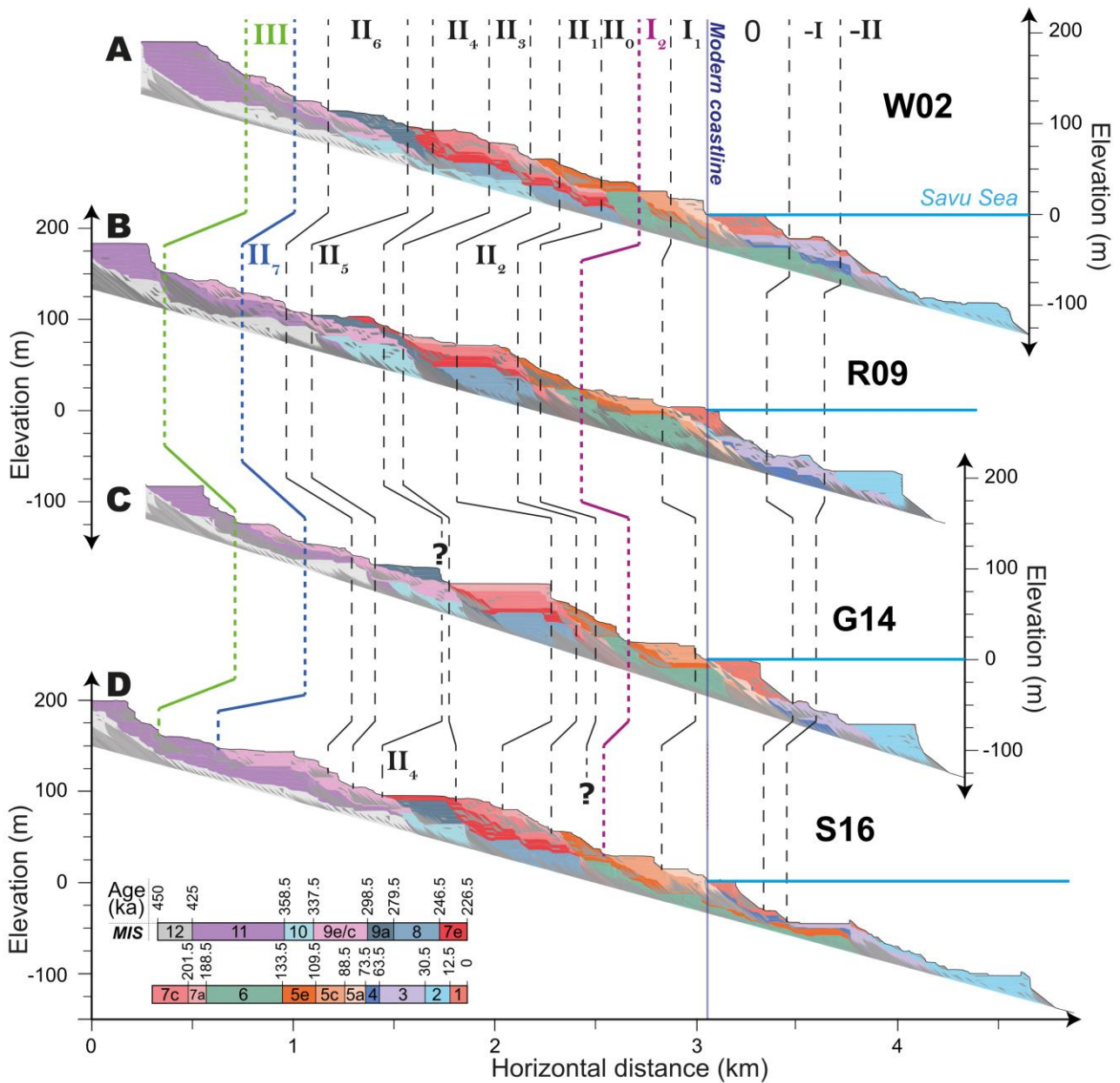
574

575 G14 (U: 0.50 mm a⁻¹; G_{max}: 6 mm a⁻¹; V: 60 mm³ a⁻¹; α: 7 %) predicts a
576 submerged barrier reef (Fig. 7C). This simulation shows a main CRT I mainly
577 constructed by a RLU associated with MIS 5c, only few parts of MIS 5e and 5a
578 RLUs outcrop. The simulated morphology of the main CRT II is globally in
579 disagreement with field measurements. For example, the simulated CRT II₃ has
580 a very "rectangular" shape and a width of more than 500 m, where field

581 measurements show a rounded morphology and a width of a few tens of meters
582 (Figs. 5A; 7C).

583

584 With S16 (U : 0.45 mm a^{-1} ; G_{max} : 6 mm a^{-1} ; E : $60 \text{ mm}^3 \text{ a}^{-1}$; α : 6%), we found
585 a morphology of main CRT II more in line with morphometric measurements
586 (Figs. 5A; 7D). However, no RLU associated with MIS 5e is outcropping on the
587 main CRT I, only two RLUs associated with MIS 5c and MIS 5a (Fig. 7D). Also,
588 this simulation does not show any submerged barrier reef, but two submerged
589 CRTs now. The model predictions obtained with W02, R09, and G14 suggest a
590 CRT at about 40 m (II_0 on profile 2; Figs. 5A; 7A; 7B; 7C), while B05 and S16
591 fail to reproduce it (Figs. 5B; 7D).



592 **Fig. 7.** Model predictions at present-day for various parametrizations (U: Uplift
593 rate; G_{max} : maximum reef growth rate; E: erosion rate; α : Initial slope) and
594 derived from the eustatic sea level curves of, **A**) Waelbroeck et al. (2002) (U:
595 0.45 mm a^{-1} ; G_{max} : 6 mm a^{-1} ; E: $60 \text{ mm}^3 \text{ a}^{-1}$; α : 6 %), **B**) Rohling et al. (2009)
596 (U: 0.46 mm a^{-1} ; G_{max} : 6 mm a^{-1} ; E: $60 \text{ mm}^3 \text{ a}^{-1}$; α : 6 %) **C**) Grant et al. (2014)
597 (U: 0.50 mm a^{-1} ; G_{max} : 6 mm a^{-1} ; E: $60 \text{ mm}^3 \text{ a}^{-1}$; α : 7 %), and **D**) Spratt and
598 Lisiecki (2016) (U: 0.45 mm a^{-1} ; G_{max} : 6 mm a^{-1} ; E: $60 \text{ mm}^3 \text{ a}^{-1}$; α : 6 %).

599

600 Finally, using a constant uplift rate (from 0.45 to 0.5 mm a⁻¹) throughout and
601 including substantial wave erosion rates (Part 3.3.), the models used herein
602 successfully predict both the age range and morphology of the highest CRT VII
603 (~470 m) at about 1 Ma (as suggested by Pirazzoli et al., 1993) as well as the
604 lower CRTs (below CRT II₁, in agreement with the dating and topographic
605 measurements; Fig. 5). This encourages us to explore in more detail how the
606 morphogenesis of diachronic lower terraces may be explained without invoking
607 any uplift rate variations (as in Bard et al., 1996).

608

609 **5. Discussion**

610

611 Here we discuss, **1)** the scenario to explain the presence of several MIS 5e
612 records at Cape Laundi, **2)** the reoccupation of the lowermost main CRT during
613 MIS 5c and 5a, and finally **3)** discuss the interactions between reef construction
614 and RSL fluctuations on the final morphology of the CRTs.

615

616 **5.1. Scenario for multiple records of MIS 5e**

617

618 Most of the best-fit simulations (all except S06) suggest at least two CRTs
619 created during MIS 5e and not necessarily during the peak of the ESL highstand
620 (Figs. 5B; 7). Several inner edges for unique ESL highstands could have formed
621 because **1)** ESL during this MIS had several peaks (e.g., Rohling et al., 2009),
622 as inferred from several CRT sequences showing double/multiple CRTs
623 associated with MIS 5e (e.g., O'Leary et al., 2013) or **2)** morphogenetic

624 processes and earlier CRTs have influenced the formation of younger reef
625 constructions.

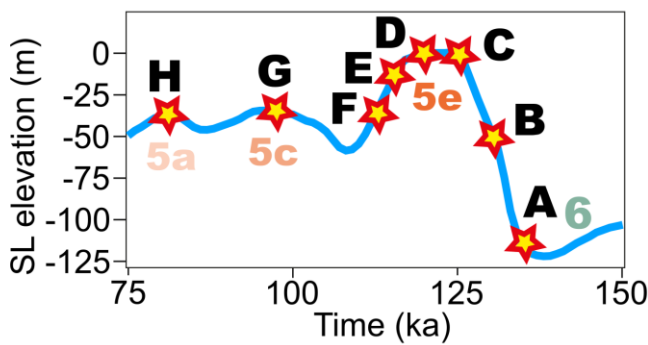
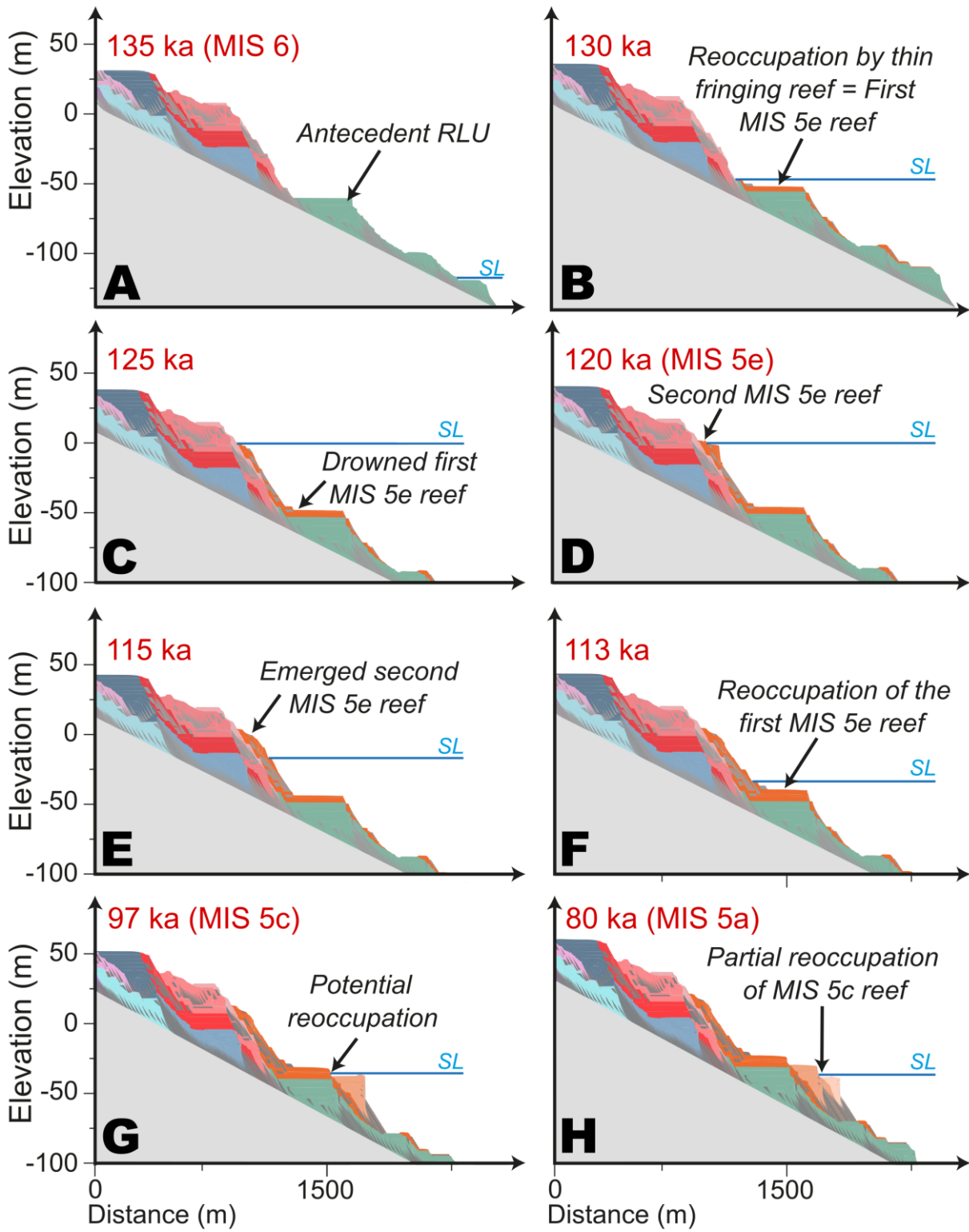
626

627 Whether ESL curves show multiple peaks (Rohling et al., 2009) or one peak
628 (Waelbroeck et al., 2002; Bintanja et al., 2005; Grant et al., 2014) during MIS
629 5e (Fig. 4), most of the simulations obtained show at least two CRTs associated
630 with MIS 5e (Figs. 5B; 7). This seems to indicate that multiple ESL or RSL peaks
631 are not required to explain the presence of several CRTs associated with MIS 5e
632 at Cape Laundi. Instead, we propose that the most likely explanation is the
633 influence of antecedent RLUs on the new ones; here, the fossil RLUs of MIS 6/7.

634

635 We unravel the development of successive RLUs from B05 by looking at
636 individual time slices of a typical model run (Fig. 8). At 130 ka, the highest CRT
637 of the MIS 6 was first reoccupied by a reef of a few meters thick (Figs. 8A, 8B).
638 This new reef was then flooded during the transgression of MIS 5e (Fig. 8C). Up
639 to 125 ka (towards the end of MIS 5e transgression), the sea slightly eroded the
640 large cliff associated with MIS 7 and thin layer of corals grew on the fossil sea
641 cliff (Fig. 8C). This was followed by the MIS 5e ESL highstand, during which a
642 reef expanded on the previous MIS 7 RLUs (Fig. 8D). The MIS 5e/5d regression
643 started at 118 ka, eroded, and slightly reoccupied the MIS 5e RLUs constructed
644 on the paleo-cliff of MIS 7 (Fig. 8E). We interpret this SL regression episode as
645 responsible for the formation of CRT II₀ (as also suggested by W02, R09, and
646 G14; Figs. 7A, 7B, 7C). At 113 ka, RSL declined to the depth of the first MIS 5e
647 RLU, itself built on the antecedent RLUs of MIS 6 (Fig. 8F). This was followed by

648 MIS 5d SL lowstand and associated RLUs on the antecedent MIS 6 constructions.



Age (ka)	298.5	279.5	246.5	226.5	201.5	188.5
MIS	9a	8	7e	7c	7a	
MIS		6	5e	5c	5a	
Age (ka)	188.5	133.5	109.5	88.5	73.5	

650 **Fig. 8.** Formation of coral reef terraces (CTRs; same simulation as in Fig. 5B
651 (B05)), at different time steps: **A)** 135, **B)** 130, **C)** 125, **D)** 120, **E)** 115, **F)** 113,
652 **G)** 97, and **H)** 80 ka ago. These time steps are placed by stars on the sea level
653 curve (from Bintanja et al., 2005) at the bottom left. At the bottom right is the
654 color scale of the CRTs associated with the Marine Isotopic Stage. The description
655 of CRTs morphogenesis can be found in sections 5.1. and 5.2..

656

657 This scenario explains the conflicting ages on the lowermost main CRT I. On CRT
658 I₁, corals have been dated at 131.5 ± 1.0 , 131.2 ± 1.0 , and 130.0 ± 1.2 ka
659 (Bard et al., 1996), indicating a reefal construction during the MIS 5e
660 transgression. On CRT I₂, corals were dated at 125.2 ± 0.9 and 124.8 ± 0.9 ka,
661 indicating a more recent reoccupation of the foundations. Alternatively, the
662 occurrence of MIS 5e age on CRT I₁ could also be explained by eroded and
663 reworked MIS 5e material during MIS 5e ESL regression or more recent ESL
664 highstands (i.e., MIS 5c and 5a). Our scenario also agrees with the only robust
665 age constraint obtained on II₁ (i.e., 129 ± 0.9 ka; Bard et al., 1996). Ages of
666 117.8 ± 1 , 113.2 ± 0.9 , or 119.3 ± 1 ka, were obtained with coral colonies
667 scattered over the main CRT I (Pirazzoli et al., 1993; Bard et al., 1996). These
668 dates indicate a reshaping and reoccupation of MIS 5e transgressive RLU during
669 MIS 5e regression.

670

671 Here, we provide an alternative scenario to the commonly used bijective
672 approach, wherein a ESL or RSL highstand is reciprocally linked to a coastal
673 terrace (see Pastier et al., 2019). We show instead that a single MIS can create

674 several CRTs and be responsible for diachronic ages on the same CRT. This is
675 mainly explained by the presence of antecedent CRTs which influence the new
676 reef constructions. Furthermore, we underline the importance of the entire SL
677 history in the generation of a CRT, and not just the highstands.

678

679 **5.2. Reoccupation during MIS 5c and 5a**

680

681 B05 does not suggest constructive reoccupation of CRT I₂ (which is associated
682 with the RSL transgression and regression of MIS 5e) during MIS 5c and 5a (Figs.
683 8G, 8H), but show a partial reoccupation of the CRT associated with MIS 5c (i.e.,
684 the most landward part of the actual CRT I₁) during MIS 5a (i.e., CRT I₁ on Fig.
685 5B; Fig. 8G). In contrast, on main CRT I, the model highlights three inner edges,
686 elevated at 22, 13, and 3 m, respectively associated with MIS 5e, 5c, and 5a
687 (Fig. 5B). Field observations show two inner edges raised at 23.2 m (CRT I₂) and
688 6.3 m (CRT I₁). Coral-colonies sampled on the CRT I₂ surface were dated at 93
689 ± 13 ka (Pirazzoli et al., 1993) and 93.4 ± 0.6 (Bard et al., 1996) and correlate
690 with MIS 5c. On CRT I₁ coral colonies provided ages of 82 ± 4 (Pirazzoli et al.,
691 1993), 86 ± 0.6 , and 107.6 ± 0.7 ka (Bard et al., 1996), which lead to the
692 interpretation that this CRT was built during MIS 5c and MIS 5a. Thus, contrary
693 to what B05 suggests, the MIS 5c and 5a RSL highstands have built RLUs now
694 above 13 m and 3 m, respectively. These simulated low elevations can be
695 explained by the fact that the ESL of MIS 5a and 5c proposed by Bintanja et al.
696 (2005) are lower than other ESL curves (e.g., W02; G14; S16; Fig. 4). Besides,
697 most simulations show a full reoccupation of the main CRT I (CRT I₁ and I₂)

698 during MIS 5c and 5a (Figs. 7A, 7B, 7C, 7D).

699

700 Considering a constant uplift of 0.5 mm a^{-1} and using recent ESL estimates of
701 $11.1 \pm 6.6 \text{ m}$ and $10.5 \pm 5.5 \text{ m}$ for MIS 5c and 5a (Creveling et al., 2017) would
702 lead to theoretical inner edge elevations of $39 \pm 7 \text{ m}$ and $31 \pm 8 \text{ m}$, respectively.
703 Thus, MIS 5c and 5a highstands could have reoccupied the entire surface of the
704 lowermost main CRT (I). This hypothesis could explain **1)** the corals dated as
705 MIS 5c on the CRT I₂ and MIS 5c and 5a on the CRT I₁ (Pirazzoli et al., 1993;
706 Bard et al., 1996) and **2)** the homogeneous ³⁶Cl cosmogenic concentrations
707 measured for the whole CRT (Chauveau et al., 2021b), interpreted as a final
708 abandonment of the surface during a single event (i.e., MIS 5c or 5a).

709

710 **5.3. Explanation of the sequence morphology**

711

712 Here, we focus on **1)** the rounded distal edges of CRTs, **2)** the influence of the
713 accommodation space on reef constructions during RSL transgressions,
714 highstands and regressions, **3)** the role of antecedent RLUs on the
715 accommodation space, and more broadly **4)** interplay between reef growth and
716 RSL changes.

717

718 The rounded shape of the CRTs distal edges leads to subtle slope ruptures
719 between adjacent CRTs and mild inner edges. We successfully reproduce these
720 landforms in our best-fit simulation (i.e., B05; Fig. 5B), as well as in W02 (Fig.
721 7A) and S16 (Fig. 7D). In contrast, simulations fail to reproduce them with G14

722 (Fig. 7C) and, to a lesser extent, with R09 (Fig. 7B). We also partly reproduce
723 the morphological differences between the main CRTs clearly separated by high
724 and steep distal parts and more subtle intermediate CRTs, especially regarding
725 CRT I and CRT II (Figs. 5A; 7A; 7B; 7D). Main CRT II is a good example of this
726 CRT morphology characterized by low sloping distal parts (Fig. 5A) forming a
727 cluster of subtle terraces. This is best reproduced with W02 (Fig. 7A), as well as
728 B05 (Fig. 5B) and S16 (Fig. 7D), poorly reproduced in R09 and not reproduced
729 in G14.

730

731 The overall rounded shape of individual CRTs is due to the low reef growth rate
732 relative to the rate of RSL change. Indeed, fast growing reefs ($G > 10 \text{ mm a}^{-1}$ in
733 our model) entirely saturate their accommodation space, thereby forming
734 "rectangular" CRT distal edges, and steeper cliffs. In this case, the
735 accommodation space is the main limiting factor acting on CRT morphology
736 (Pastier et al., 2019). Contrarily, due to the low reef growth rate in our best-fit
737 simulations for each ESL reconstructions, reef growth is typically not limited by
738 its accommodation space, neither for backstepping and catch-up during RSL rise,
739 nor for keep-up and progradation during a RSL highstand (see definitions in
740 Neumann (1985) and in Camoin and Webster (2015)). Indeed, during most
741 transgressions, the low reef growth rate is outpaced by the rate of RSL rise,
742 leading to backstepping and drowning of the reef (as the transgression of MIS
743 9a for CRT II₆ in W02; Figs. 4; 7A). The duration of RSL highstands does not
744 allow the reef to entirely fill its accommodation space and form large and flat
745 platforms. Consequently, accommodation space is still available for significant

746 reef construction during regressions, unlike fast growing reefs which mainly
747 expand during transgressions (Husson et al., 2018). Construction during RSL fall
748 leads to seaward sloping CRTs surfaces (e.g., CRT II₁, II₃, II₄, II₅, II₆ in Fig. 5A),
749 particularly well expressed in B05 (Fig. 5B), S16, W02, and R09, but not in G14
750 (Fig. 7). Thus, the absence of clearly marked fossil sea-cliffs and notches in the
751 distal part of most of the CRTs in the Cape Laundi sequence, but also their
752 roundness, is plausible evidence of a last episode of construction during RSL
753 regression.

754

755 Also, reef construction during reoccupations of antecedent RLUs associated with
756 MIS highstands may cover the shoreline angle of antecedent CRTs, leading to
757 missing terraces (e.g., CRT II₄ in Fig. 7C). But these antecedent CRTs also
758 provide the reef with a larger accommodation space, which fosters the
759 development of large and flat CRTs. For example, in our study, ESL
760 reconstructions providing higher elevations for MIS 7c highstand relative to MIS
761 7a (i.e., W02, B05, and S16) show more realistic morphologies than ESL
762 reconstructions with lower relative elevation for the MIS 7c highstand (R09 and
763 G14). With G14 (Fig. 7C), the multiple reoccupations of RLUs constructed during
764 MIS 8, 7e and 7c lead to the formation of the widest and flattest CRT of the
765 sequence (~514 m, CRT II₃ in Fig. 7C). Similarly, the relatively high SL of MIS
766 9a in the ESL reconstruction of Waelbroeck et al. (2002) (Fig. 4) prevents any
767 reoccupation on CRT II₆ during MIS 7e (Fig. 7A), despite the slightly lower uplift
768 rate (Fig. 6). Both R09 and G14 exhibit a greater difference between the
769 elevations of these highstands compared to that of W02. This greater difference

770 in elevation leads to the coincidence of final relative elevation for MIS 9a and
771 MIS 7e, resulting in the formation of a composite but not compound terrace
772 when modeling with R09 (CRT II₅ in Fig. 7B; Fig. 2). G14 does not show such a
773 composite terrace (Fig. 7C). The accommodation space during the MIS 7e final
774 transgression and highstand is very small due to the former construction of RLU
775 during MIS 9a. Thus, reefal construction is limited during MIS 7e, and the RLU
776 associated with this MIS finally eroded during the following regression. This
777 explains why there is no geomorphic record of the MIS 7e highstand within the
778 final sequence of G14 (Fig. 7C and Supplementary Animation S4). Therefore,
779 the rounded morphology of the intermediate CRTs composing the main CRT II
780 can be explained by the relative elevation of the ESL highstands.

781

782 The morphology of the seaward part of CRT IV (associated with MIS 11) is
783 successfully reproduced in W02 (Fig. 7A) and B05 (Fig. 5B). In the other
784 simulations, the distal part of this main CRT is too steep (Fig. 7B) and exhibit
785 well individualized terraces (Figs. 7C, 7D). There are also MIS 11 constructions
786 on CRT III, partly for R09 (Fig. 7B) and for the entire CRT with S16 (Fig. 7D).
787 Similarly, the morphology of CRT IV in our simulations would results from the
788 feedbacks between RSL variations and the low reef growth rate. The rate of RSL
789 rise after 425 ka (Fig. 4) is slightly higher than the effective reef growth rate.
790 This induces a catch-up growth regime (Neumann, 1985), preventing
791 construction along the whole reef flat and resulting in a migration of the reef
792 crest landward (Fig. 7A and Supplementary Animation S2). Then, the long
793 duration of the highstand results in an increased supply of clastic sediments to

794 the forereef slope, smoothing the slope. Finally, because the accommodation
795 space hasn't been saturated during the previous transgression and highstand, a
796 narrow fringing reef can construct a thin veneer of limestone all along the slow
797 regression, covering the clastic sediments of the forereef slope. Using other ESL
798 reconstructions, the average rates of RSL rise are either low enough to allow the
799 reef to keep-up, and to form a steep forereef slope (Fig. 7B, Supplementary
800 Animation S3; Fig. 7C, Supplementary Animation S4) or too high and lead to the
801 backstepping of the reef (Fig. 7D, Supplementary Animation S5). Then, all ESL
802 reconstructions of MIS 11 used here (Fig. 4) show second order ESL rises or ESL
803 stagnations, which carve and steepen up the distal part of CRT IV. This can even
804 lead to the formation of extra terraces on the CRT IV distal part, which may be
805 purely erosive, as in W02, G14 and S16 (Figs. 7A, 7C, 7D).

806

807 The discussion above serves to illustrate that specific ESL reconstructions lead
808 to specific morphological features that may, or may not, match with observations
809 and dating of CRTs. In a general sense, this study shows that careful modeling
810 the morphology of a CRTs sequence permits to unravel the rates of past SL
811 variations, to better understand the bioconstruction formed during
812 transgressions, highstands and regression, and thus potentially to improve SL
813 reconstructions of these fluctuations. This study only focuses on one site and
814 therefore any inferences on global SL reconstructions may be biased by local
815 peculiarities at Cape Laundi (e.g., erosive and constructive reoccupation
816 processes, Chauveau et al., 2021b), but a similar approach may be applied to
817 other sites with double/multiple CRT outcrops associated with MIS 5e (e.g.,

818 Hearty et al., 2007). A comprehensive comparison of several such sequences
819 may eventually lead to improved SL reconstructions on a global level.

820

821 **6. Conclusions**

822

823 The long-lasting CRT sequence of Cape Laundi has the potential to serve as a
824 crucial archive for studies of Quaternary sea level oscillations. However, until
825 now, the diachronism and the composite nature of coral reef terraces challenged
826 any bijective, or reciprocal, association of a terrace with a discrete sea level
827 highstand. To address this, on the basis of a chrono-morphological study of 625
828 simulations from a kinematic model based on reef morphology, testing five sea
829 level curves, we were able to **1)** constrain the parameters that generated the
830 sequence (i.e., uplift rate, reef growth rate, erosion rate, and slope of
831 foundations), **2)** explain the presence of MIS 5e ages of corals sampled on three
832 distinct terraces by retracing the eustatic history of this MIS and by
833 demonstrating that it is not necessary to invoke a double sea level peak, **3)**
834 unravel the formation of composite coral reef terraces by highlighting
835 reoccupation during MIS 5c and 5a, **4)** explain the rounded morphology of
836 terrace distal edges at Cape Laundi with the low reef growth rate, and **5)** discuss
837 the interactions between reef construction and relative sea level fluctuations on
838 the final morphology of the terraces. Careful modeling can therefore explain the
839 morphology of a sequence of coral reef terraces and, to a greater extent, discuss
840 precisely the processes that generated it.

841

842 **ACKNOWLEDGEMENTS**

843

844 *This work was supported by public funds received of the program*
845 *"Investissements d'Avenir" managed by the French National Research Agency*
846 *(ANR-10-EQPX-20 and ANR-10-LABX-19-01, Labex Mer, CLIMORESO, C.*
847 *Authemayou), the INSU Tellus Syster program (SECOMAS, C. Authemayou), and*
848 *the CNES TOSCA program (CETTROPICO, C. Authemayou). We thank the State*
849 *Ministry of Research and Technology of Indonesia "KEMENRISTEK" that allowed*
850 *us to conduct the field trip to Sumba (research permit*
851 *680/FRP/E5/Dit.KI/IV/2017). We also thank Dr. Danny Hilman Natawidjaja and*
852 *Vera Christanti Agusta for their help during the fieldwork. Finally, we thank David*
853 *Fernández Blanco for the stacked swath profiles.*

854

855 **References**

856

- 857 **1.** Abdullah, C. I., Rampnoux, J. P., Bellon, H., Maury, R. C., & Soeria-
858 Atmadja, R. (2000). The evolution of Sumba Island (Indonesia) revisited
859 in the light of new data on the geochronology and geochemistry of the
860 magmatic rocks. *Journal of Asian Earth Sciences*, 18(5), 533-546.
- 861
- 862 **2.** Anderson, R. S., Densmore, A. L., & Ellis, M. A. (1999). The generation
863 and degradation of marine terraces. *Basin Research*, 11(1), 7-20.

864

- 865 **3.** Armijo, R., Lacassin, R., Coudurier-Curveur, A., & Carrizo, D. (2015). Cou-
866 pled tectonic evolution of Andean orogeny and global climate. *Earth-Sci-*
867 *ence Reviews*, 143, 1–35.
- 868
- 869 **4.** Authemayou, C., Brocard, G., Delcaillau, B., Molliex, S., Pedoja, K., Hus-
870 son, L., et al. (2018). Unraveling the roles of asymmetric uplift, normal
871 faulting and groundwater flow to drainage rearrangement in an emerging
872 karstic landscape. *Earth Surface Processes and Landforms*, 43(9), 1885-
873 1898.
- 874
- 875 **5.** Authemayou, C., Pedoja, K., Chauveau, D., Husson, L., Brocard, G.,
876 Delcaillau, B., ... & Scholz, D. (2022). Deformation and uplift at the tran-
877 sition from oceanic to continental subduction, Sumba Island, Indonesia.
878 *Journal of Asian Earth Sciences*, 236, 105316.
- 879
- 880 **6.** Bard, E., Jouannic, C., Hamelin, B., Pirazzoli, P., Arnold, M., Faure, G., et
881 al. (1996). Pleistocene sea levels and tectonic uplift based on dating of
882 corals from Sumba Island, Indonesia. *Geophysical Research Letters*,
883 23(12), 1473-1476.
- 884
- 885 **7.** Bintanja, R., Van De Wal, R. S. W., & Oerlemans, J. (2005). Modelled at-
886 mospheric temperatures and global sea levels over the past million years.
887 *Nature*, 437(7055), 125-128.
- 888

- 889 **8.** Bosscher, H., & Schlager, W. (1992). Computer simulation of reef growth.
890 *Sedimentology*, 39(3), 503-512.
891
- 892 **9.** Boulton, S. J., & Stokes, M. (2018). Which DEM is best for analyzing fluvial
893 landscape development in mountainous terrains?. *Geomorphology*, 310,
894 168-187.
895
- 896 **10.** Broecker, W. S., & Thurber, D. L. (1965). Uranium-series dating of
897 corals and oolites from Bahaman and Florida Key limes-
898 tones. *Science*, 149(3679), 58-60.
899
- 900 **11.** Cabioch, G. (2011). Emerged reefs. *Encyclopedia of Modern Coral*
901 *Reefs: Structure, Form and Process*, 373-380.
902
- 903 **12.** Camoin, G. F., & Webster, J. M. (2015). Coral reef response to Qua-
904 ternary sea-level and environmental changes: State of the science. *Sedi-*
905 *mentology*, 62(2), 401-428.
906
- 907 **13.** Caputo, R. (2007). Sea-level curves: perplexities of an end-user in
908 morphotectonic applications. *Global and Planetary Change*, 57(3-4), 417-
909 423.
910

- 911 **14.** Chappell, J. (1974). Geology of coral terraces, Huon Peninsula, New
912 Guinea: a study of Quaternary tectonic movements and sea-level changes.
913 Geological Society of America Bulletin, 85(4), 553-570.
914
- 915 **15.** Chappell, J. (1980). Coral morphology, diversity and reef
916 growth. Nature, 286(5770), 249-252.
917
- 918 **16.** Chauveau, D., Authemayou, C., Molliex, S., Godard, V., Benedetti,
919 L., Pedoja, K., ... & ASTER Team. (2021a). Eustatic knickpoint dynamics
920 in an uplifting sequence of coral reef terraces, Sumba Island, Indone-
921 sia. *Geomorphology*, 393, 107936.
922
- 923 **17.** Chauveau, D., Authemayou, C., Pedoja, K., Molliex, S., Husson, L.,
924 Scholz, D., ... & ASTER Team. (2021b). On the generation and degradation
925 of emerged coral reef terrace sequences: First cosmogenic ³⁶Cl analysis
926 at Cape Laundi, Sumba Island (Indonesia). *Quaternary Science Re-
927 views*, 269, 107144.
928
- 929 **18.** Creveling, J. R., Mitrovica, J. X., Clark, P. U., Waelbroeck, C., & Pico,
930 T. (2017). Predicted bounds on peak global mean sea level during marine
931 isotope stages 5a and 5c. *Quaternary Science Reviews*, 163, 193-208.
932
- 933 **19.** Crosby, W. O. (1883). Elevated coral reefs of cuba. *Journal of Natu-
934 ral History*, 12(70), 283-284.

935

936 **20.** Darwin, C. (1842). The Structure and Distribution of Coral Reefs:
937 Being the First Part of the Geology of the Voyage of the Beagle... During
938 the Years 1832-1836: Smith, Elder.

939

940 **21.** de Gelder, G., Jara-Muñoz, J., Melnick, D., Fernández-Blanco, D.,
941 Rouby, H., Pedroja, K., Husson, L., Armijo, R., & Lacassin, R. (2020). How
942 do sea-level curves influence modeled marine terrace sequences? Quater-
943 nary Science Reviews, 229, 106132.

944

945 **22.** de Gelder, G., Husson, L., Pastier, A. M., Fernández-Blanco, D., Pico,
946 T., Chauveau, D., ... & Pedroja, K. (2022). High interstadial sea levels over
947 the past 420ka from the Huon Peninsula, Papua New Guinea. Communi-
948 cations Earth & Environment, 3(1), 256.

949

950 **23.** Delanghe, D., Bard, E., & Hamelin, B. (2002). New TIMS constraints
951 on the uranium-238 and uranium-234 in seawaters from the main ocean
952 basins and the Mediterranean Sea. *Marine Chemistry*, 80(1), 79-93.

953

954 **24.** Elderfield, H., Ferretti, P., Greaves, M., Crowhurst, S., McCave, I. N.,
955 Hodell, D., et al. (2012). Evolution of ocean temperature and ice volume
956 through the mid-Pleistocene climate transition. *Science*, 337(6095), 704-
957 709.

958

- 959 **25.** Fernández-Blanco, D., de Gelder, G., Lacassin, R., & Armijo, R.
960 (2019). Geometry of flexural uplift by continental rifting in Corinth,
961 Greece. *Tectonics*. <https://doi.org/10.1029/2019TC005685>
962
- 963 **26.** Fleury, J.-M., Pubellier, M., & de Urreiztieta, M. (2009). Structural
964 expression of forearc crust uplift due to subducting asperity. *Lithos*, 113(1-
965 2), 318-330.
966
- 967 **27.** Fortuin, A. R., Van der Werff, W., & Wensink, H. (1997). Neogene
968 basin history and paleomagnetism of a rifted and inverted forearc region,
969 on-and offshore Sumba, Eastern Indonesia. *Journal of Asian Earth Sci-*
970 *ences*, 15(1), 61-88.
971
- 972 **28.** Grant, K. M., Rohling, E. J., Ramsey, C. B., Cheng, H., Edwards, R.
973 L., Florindo, F., et al. (2014). Sea-level variability over five glacial cycles.
974 *Nature communications*, 5(1), 1-9.
975
- 976 **29.** Haig, D. W. (2012). Palaeobathymetric gradients across Timor dur-
977 ing 5.7-3.3 Ma (latest Miocene-Pliocene) and implications for collision up-
978 lift. *Palaeogeography, Palaeoclimatology, Palaeoecology*, 331, 50-59.
979
- 980 **30.** Hantoro, W. S., Jouannic, C., & Pirazzoli, P. A. (1989). Terrasses
981 coralliennes quaternaires soulevées dans l'île de Sumba (Indonésie). *Photo*
982 *interprétation (Paris)*, 28(1), 17-34.

983

984 **31.** Hantoro, W. S. (1992). Etude des terrasses récifales Quaternaires
985 soulevées entre le Détroit de la Sonde et l'île de Timor, Indonésie: mou-
986 vements verticaux de la croûte terrestre et variations du niveau de la mer.

987

988 **32.** Hearty, P. J., Hollin, J. T., Neumann, A. C., O'Leary, M. J., & McCul-
989 loch, M. (2007). Global sea-level fluctuations during the Last Interglacia-
990 tion (MIS 5e). *Quaternary Science Reviews*, 26(17-18), 2090-2112.

991

992 **33.** Hirschberger, F., Malod, J.-A., Réhault, J.-P., Villeneuve, M., Royer,
993 J.-Y., & Burhanuddin, S. (2005). Late Cenozoic geodynamic evolution of
994 eastern Indonesia. *Tectonophysics*, 404(1-2), 91-118.

995

996 **34.** Hume, W. F., & Little, O. H. (1928). Raised beaches and terraces of
997 Egypt. *Union Geograph. Intern., Paris, Rept. Comm. Plio-Pleist. Terraces*,
998 9-15.

999

1000 **35.** Husson, L., Pastier, A.-M., Pedoja, K., Elliot, M., Paillard, D., Au-
1001 themayou, C., et al. (2018). Reef carbonate productivity during Quater-
1002 nary sea level oscillations. *Geochemistry, Geophysics, Geosystems*, 19(4),
1003 1148-1164.

1004

1005 **36.** Husson, L., Riel, N., Aribowo, S., Authemayou, C., de Gelder, G.,
1006 Kaus, B. J. P., ... & Sarr, A. C. (2022). Slow geodynamics and fast

1007 morphotectonics in the far East Tethys. *Geochemistry, Geophysics, Ge-*
1008 *osystems*, 23(1), e2021GC010167.

1009

1010 **37.** Jouannic, C., Hantoro, W. S., Hoang, C. T., Fournier, M., Lafont, R.,
1011 & Ichtam, M. L. (1988). Quaternary raised reef terraces at cape Laundi,
1012 Sumba, Indonesia: geomorphological analysis and first radiometric Th/U
1013 and 14C age determinations. Paper presented at the 6th Proceedings In-
1014 ternational coral reef symposium.

1015

1016 **38.** Koelling, M., Webster, J. M., Camoin, G., Iryu, Y., Bard, E., & Seard,
1017 C. (2009). SEALEX-Internal reef chronology and virtual drill logs from a
1018 spreadsheet-based reef growth model. *Global and Planetary Change*,
1019 66(1-2), 149-159.

1020

1021 **39.** Lazar, B., Enmar, R., Schossberger, M., Bar-Matthews, M., Halicz,
1022 L., & Stein, M. (2004). Diagenetic effects on the distribution of uranium in
1023 live and Holocene corals from the Gulf of Aqaba. *Geochimica et Cosmochi-*
1024 *mica Acta*, 68(22), 4583-4593.

1025

1026 **40.** Murray-Wallace, C. V., & Woodroffe, C. D. (2014). Quaternary sea-
1027 level changes: a global perspective: Cambridge University Press.

1028

1029 **41.** Neumann, A. C. (1985). Reef response to sea-level rise: keep-up,
1030 catch-up, or give-up. In *Proceedings of the fifth international coral reef*

1031 congress Tahiti, 27 May-1 June 1985 volume 3: Symposia and seminars
1032 (A) (pp. 105-110). Antenne Museum-EPHE.

1033

1034 **42.** Nexer, M., Authemayou, C., Schildgen, T., Hantoro, W. S., Molliex,
1035 S., Delcaillau, B., et al. (2015). Evaluation of morphometric proxies for
1036 uplift on sequences of coral reef terraces: A case study from Sumba Island
1037 (Indonesia). *Geomorphology*, 241, 145-159.

1038

1039 **43.** O'Leary, M. J., Hearty, P. J., Thompson, W. G., Raymo, M. E., Mi-
1040 trovica, J. X., & Webster, J. M. (2013). Ice sheet collapse following a pro-
1041 longed period of stable sea level during the last interglacial. *Nature Geos-
1042 cience*, 6(9), 796-800.

1043

1044 **44.** Obert, J. C., Scholz, D., Felis, T., Brocas, W. M., Jochum, K. P., &
1045 Andreae, M. O. (2016). ²³⁰Th/U dating of Last Interglacial brain corals
1046 from Bonaire (southern Caribbean) using bulk and theca wall material.
1047 *Geochimica et Cosmochimica Acta*, 178, 20-40.

1048

1049 **45.** Obert, J. C., Scholz, D., Felis, T., Lippold, J., Jochum, K. P., & An-
1050 dreae, M. O. (2019). Improved constraints on open-system processes in
1051 fossil reef corals by combined Th/U, Pa/U and Ra/Th dating: A case study
1052 from Aqaba, Jordan. *Geochimica et Cosmochimica Acta*, 245, 459-478.

1053

- 1054 **46.** Pastier, A.-M., Husson, L., Pedoja, K., Bézos, A., Authemayou, C.,
1055 Arias-Ruiz, C., et al. (2019). Genesis and Architecture of Sequences of
1056 Quaternary Coral Reef Terraces: Insights From Numerical Models. *Geo-*
1057 *chemistry, Geophysics, Geosystems*.
- 1058
- 1059 **47.** Pedoja, K., Husson, L., Regard, V., Cobbold, P. R., Ostancaux, E.,
1060 Johnson, M. E., et al. (2011). Relative sea-level fall since the last intergla-
1061 cial stage: are coasts uplifting worldwide? *Earth-Science Reviews*, 108(1-
1062 2), 1-15.
- 1063
- 1064 **48.** Pedoja, K., Husson, L., Johnson, M. E., Melnick, D., Witt, C., Pochat,
1065 S., et al. (2014). Coastal staircase sequences reflecting sea-level oscilla-
1066 tions and tectonic uplift during the Quaternary and Neogene. *Earth-Sci-*
1067 *ence Reviews*, 132, 13-38.
- 1068
- 1069 **49.** Pedoja, K., Husson, L., Bezos, A., Pastier, A.-M., Imran, A. M., Arias-
1070 Ruiz, C., et al. (2018). On the long-lasting sequences of coral reef terraces
1071 from SE Sulawesi (Indonesia): Distribution, formation, and global signifi-
1072 cance. *Quaternary Science Reviews*, 188, 37-57.
- 1073
- 1074 **50.** Peñalver, L., Pedoja, K., Martin-Izquierdo, D., Authemayou, C.,
1075 Nuñez, A., Chauveau, D., ... & Husson, L. (2021). The Cuban staircase
1076 sequences of coral reef and marine terraces: A forgotten masterpiece of
1077 the Caribbean geodynamical puzzle. *Marine Geology*, 440, 106575.

1078

1079 **51.** Pirazzoli, P. A. (2005). A review of possible eustatic, isostatic and
1080 tectonic contributions in eight late-Holocene relative sea-level histories
1081 from the Mediterranean area. *Quaternary Science Reviews*, 24(18-19),
1082 1989-2001.

1083

1084 **52.** Pirazzoli, P. A., Radtke, U., Hantoro, W. S., Jouannic, C., Hoang, C.
1085 T., Causse, C., et al. (1991). Quaternary raised coral-reef terraces on
1086 Sumba Island, Indonesia. *Science*, 252(5014), 1834-1836.

1087

1088 **53.** Pirazzoli, P. A., Radtke, U., Hantoro, W. S., Jouannic, C., Hoang, C.
1089 T., Causse, C., et al. (1993). A one million-year-long sequence of marine
1090 terraces on Sumba Island, Indonesia. *Marine Geology*, 109(3-4), 221-236.

1091

1092 **54.** Railsback, L. B., Gibbard, P. L., Head, M. J., Voarintsoa, N. R. G., &
1093 Toucanne, S. (2015). An optimized scheme of lettered marine isotope sub-
1094 stages for the last 1.0 million years, and the climatostratigraphic nature
1095 of isotope stages and substages. *Quaternary Science Reviews*, 111, 94-
1096 106.

1097

1098 **55.** Robinson, L. F., Henderson, G. M., Hall, L., & Matthews, I. (2003,
1099 December). Controls on $\delta^{234}\text{U}$ in surface waters of the South Island of
1100 New Zealand. In *AGU Fall Meeting Abstracts* (Vol. 2003, pp. V51C-0306).

1101

- 1102 **56.** Rohling, E. J., Grant, K., Bolshaw, M., Roberts, A. P., Siddall, M.,
1103 Hemleben, C., et al. (2009). Antarctic temperature and global sea level
1104 closely coupled over the past five glacial cycles. *Nature Geoscience*, 2(7),
1105 500-504.
- 1106
- 1107 **57.** Rohling, E. J., Foster, G. L., Grant, K. M., Marino, G., Roberts, A. P.,
1108 Tamisiea, M. E., & Williams, F. (2014). Sea-level and deep-sea-tempera-
1109 ture variability over the past 5.3 million years. *Nature*, 508(7497), 477-
1110 482.
- 1111
- 1112 **58.** Rovere, A., Stocchi, P. & Vacchi, M. Eustatic and Relative Sea Level
1113 Changes. *Curr Clim Change Rep* **2**, 221–231 (2016a).
1114 <https://doi.org/10.1007/s40641-016-0045-7>
- 1115
- 1116 **59.** Rovere, A., Raymo, M. E., Vacchi, M., Lorscheid, T., Stocchi, P.,
1117 Gomez-Pujol, L., et al. (2016b). The analysis of Last Interglacial (MIS 5e)
1118 relative sea-level indicators: Reconstructing sea-level in a warmer world.
1119 *Earth-Science Reviews*, 159, 404-427.
- 1120
- 1121 **60.** Rupnik, E., Deseilligny, M. P., Delorme, A., & Klinger, Y. (2016). Re-
1122 fined satellite image orientation in the free open-source photogrammetric
1123 tools Apero/Micmac. *ISPRS Annals of the Photogrammetry, Remote Sens-*
1124 *ing and Spatial Information Sciences*, 3, 83.

1125

- 1126 **61.** Scholz, D., Mangini, A., & Felis, T. (2004). U-series dating of diage-
1127 netically altered fossil reef corals. *Earth and Planetary Science Letters*,
1128 218(1-2), 163-178.
- 1129
- 1130 **62.** Schwartz, M. (2006). *Encyclopedia of coastal science*: Springer Sci-
1131 ence & Business Media.
- 1132
- 1133 **63.** Shakun, J. D., Lea, D. W., Lisiecki, L. E., & Raymo, M. E. (2015). An
1134 800-kyr record of global surface ocean $\delta^{18}O$ and implications for ice vol-
1135 ume-temperature coupling. *Earth and Planetary Science Letters*, 426, 58-
1136 68.
- 1137
- 1138 **64.** Sosdian, S., & Rosenthal, Y. (2009). Deep-sea temperature and ice
1139 volume changes across the Pliocene-Pleistocene climate transitions. *Sci-*
1140 *ence*, 325(5938), 306-310.
- 1141
- 1142 **65.** Speed, R. C., & Cheng, H. (2004). Evolution of marine terraces and
1143 sea level in the last interglacial, Cave Hill, Barbados. *Geological Society of*
1144 *America Bulletin*, 116(1-2), 219-232.
- 1145
- 1146 **66.** Spratt, R. M., & Lisiecki, L. E. (2016). A Late Pleistocene sea level
1147 stack. *Climate of the Past*, 12(4), 1079-1092.
- 1148

- 1149 **67.** Tate, G. W., McQuarrie, N., van Hinsbergen, D. J., Bakker, R. R.,
1150 Harris, R., Willett, S., ... & Zachariasse, W. J. (2014). Resolving spatial
1151 heterogeneities in exhumation and surface uplift in Timor - Leste: Con-
1152 traints on deformation processes in young orogens. *Tectonics*, 33(6),
1153 1089-1112.
- 1154
- 1155 **68.** Thompson, W. G., & Goldstein, S. L. (2005). Open-system coral ages
1156 reveal persistent suborbital sea-level cycles. *Science*, 308(5720), 401-
1157 404.
- 1158
- 1159 **69.** Toomey, M., Ashton, A. D., & Perron, J. T. (2013). Profiles of ocean
1160 island coral reefs controlled by sea-level history and carbonate accumula-
1161 tion rates. *Geology*, 41(7), 731-734.
- 1162
- 1163 **70.** Turcotte, D. L., & Bernthal, M. J. (1984). Synthetic coral-reef ter-
1164 races and variations of Quaternary sea level. *Earth and Planetary Science*
1165 *Letters*, 70(1), 121-128.
- 1166
- 1167 **71.** Waelbroeck, C., Labeyrie, L., Michel, E., Duplessy, J. C., McManus,
1168 J. F., Lambeck, K., et al. (2002). Sea-level and deep water temperature
1169 changes derived from benthic foraminifera isotopic records. *Quaternary*
1170 *Science Reviews*, 21(1-3), 295-305.
- 1171

1172 **72.** Webster, J. M., Wallace, L. M., Clague, D. A., & Braga, J. C. (2007).
1173 Numerical modeling of the growth and drowning of Hawaiian coral reefs
1174 during the last two glacial cycles (0-250 kyr). *Geochemistry, Geophysics,*
1175 *Geosystems*, 8(3).

1176

1177

1178

1179

1180

1181

1182

1183

1184

1185

1186

1187

1188

1189

1190

1191

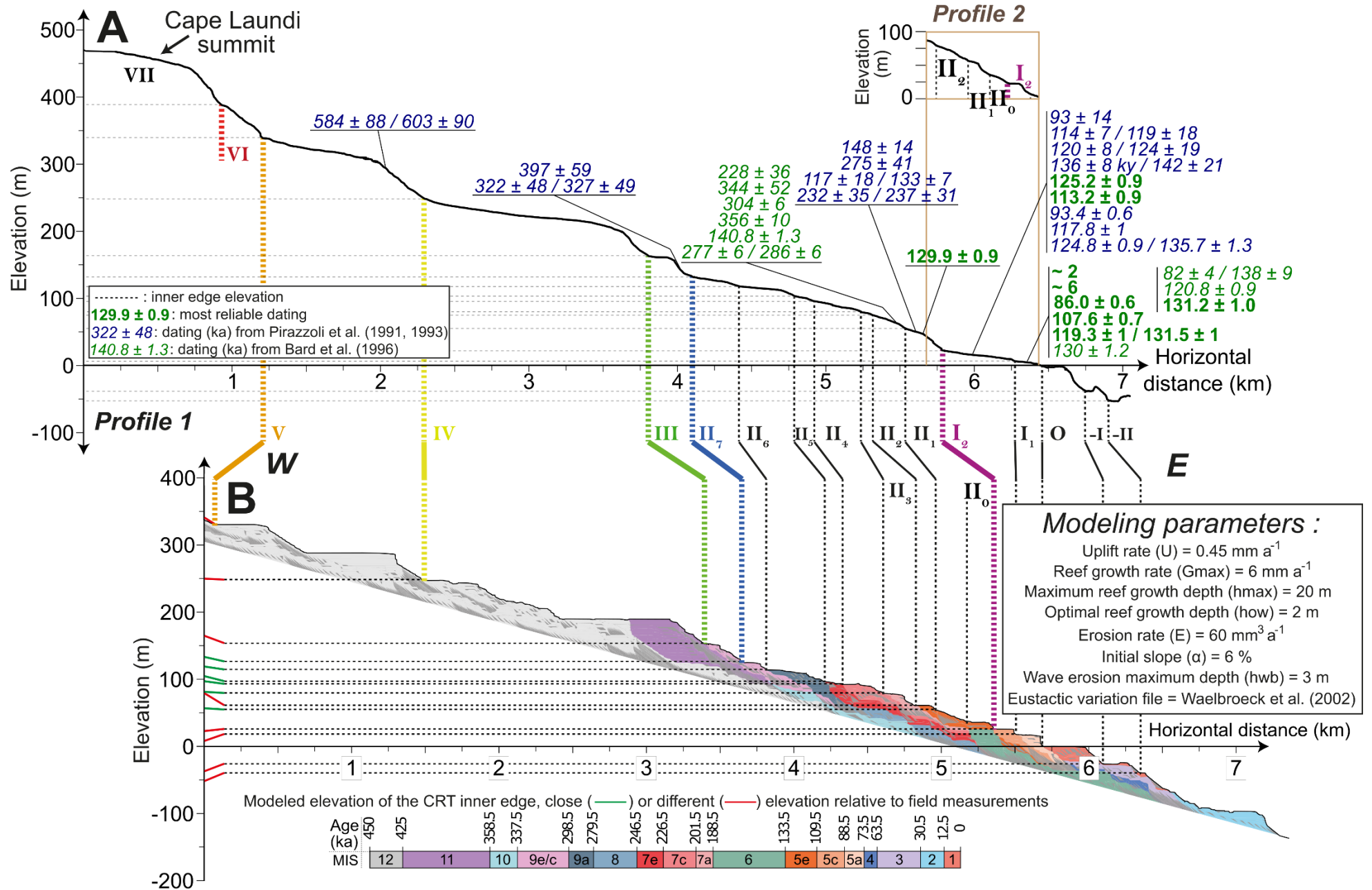
1192

1193

1194

1195

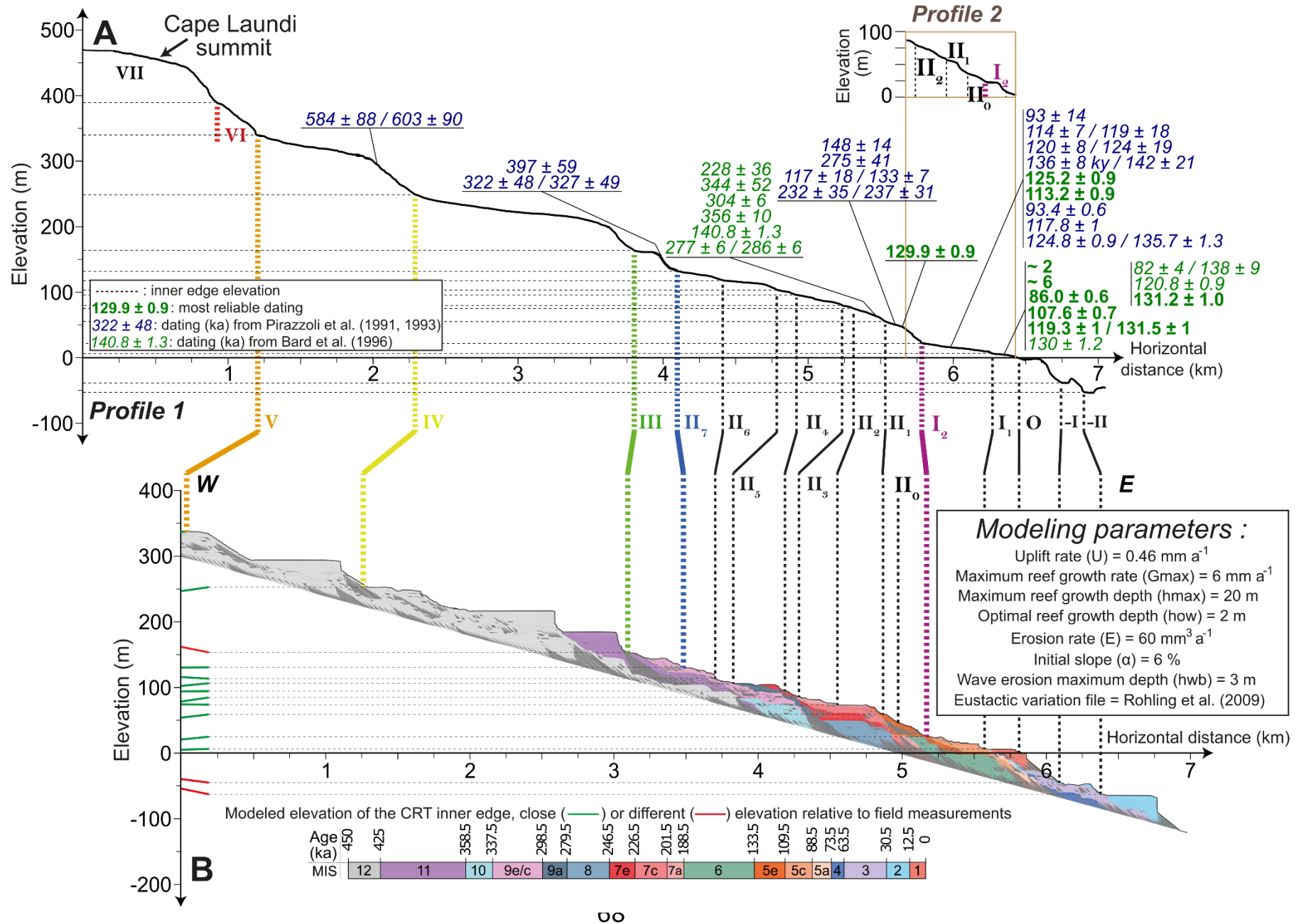
Supporting information



1198

1199 **Supporting Information - W02**

1200 **A)** Morphometric profiles (dGPS and sonar) at Cape Laundi, showing the location and ages of U/Th and Electron spin
1201 resonance (ESR) samples (Pirazzoli et al., 1991, 1993; Bard et al., 1996). **B)** Best-fit numerical simulation from the
1202 sea level reconstruction of Waelbroeck et al., (2002), i.e., W02; U (uplift rate): 0.45 mm a^{-1} ; G_{max} (maximum reef
1203 growth rate): 6 mm a^{-1} ; E (erosion rate): $60 \text{ mm}^3 \text{ a}^{-1}$; α (initial slope): 6 %). The red and green lines (near the y-
1204 axis) show the modeled elevations of the coral reef terrace (CRT) inner edges, close to or different from field
1205 measurements, respectively.

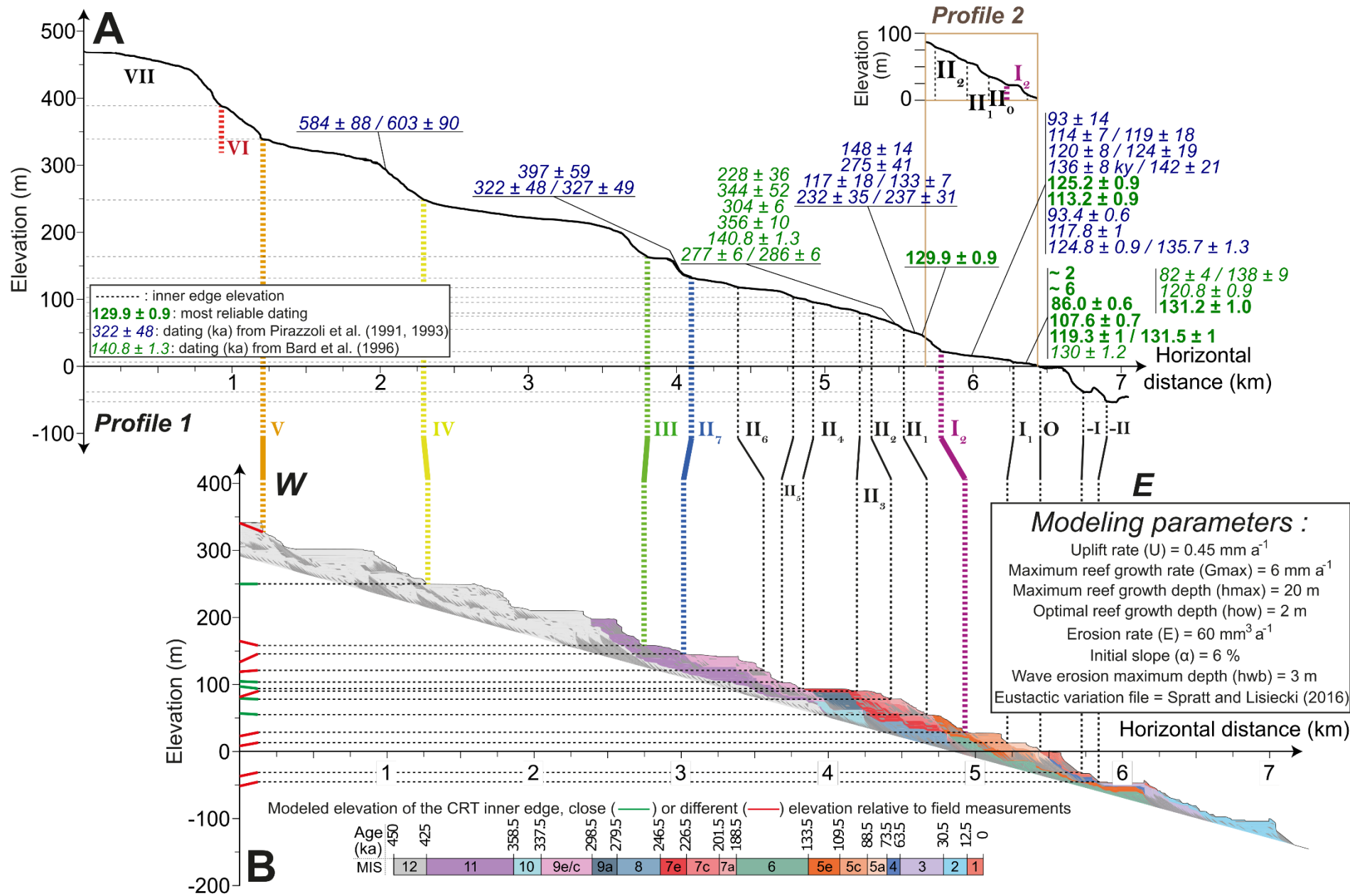


1207 **Supporting Information - R09**

1208 **A)** Morphometric profiles (dGPS and sonar) at Cape Laundi, showing the location and ages of U/Th and Electron spin
1209 resonance (ESR) samples (Pirazzoli et al., 1991, 1993; Bard et al., 1996). **B)** Best-fit numerical simulation from the
1210 sea level reconstruction of Rohling et al., (2009), i.e., R09; U (uplift rate): 0.46 mm a^{-1} ; G_{max} (maximum reef growth
1211 rate): 6 mm a^{-1} ; E (erosion rate): $60 \text{ mm}^3 \text{ a}^{-1}$; α (initial slope): 6 %). The red and green lines (near the y-axis) show
1212 the modeled elevations of the coral reef terrace (CRT) inner edges, close to or different from field measurements,
1213 respectively.

1215 **Supporting Information - G14**

1216 **A)** Morphometric profiles (dGPS and sonar) at Cape Laundi, showing the location and ages of U/Th and Electron spin
1217 resonance (ESR) samples (Pirazzoli et al., 1991, 1993; Bard et al., 1996). **B)** Best-fit numerical simulation from the
1218 sea level reconstruction of Grant et al., (2014), i.e., G14; U (uplift rate): 0.50 mm a⁻¹; G_{max} (maximum reef growth
1219 rate): 6 mm a⁻¹; E (erosion rate): 60 mm³ a⁻¹; α (initial slope): 7 %. The red and green lines (near the y-axis) show
1220 the modeled elevations of the coral reef terrace (CRT) inner edges, close to or different from field measurements,
1221 respectively.



1223

1224 **Supporting Information - S16**

1225 **A)** Morphometric profiles (dGPS and sonar) at Cape Laundi, showing the location
1226 and ages of U/Th and Electron spin resonance (ESR) samples (Pirazzoli et al.,
1227 1991, 1993; Bard et al., 1996). **B)** Best-fit numerical simulation from the sea
1228 level reconstruction of Spratt and Lisiecki (2016), i.e., S16; U (uplift rate): 0.45
1229 mm a⁻¹; G_{max} (maximum reef growth rate): 6 mm a⁻¹; E (erosion rate): 60 mm³
1230 a⁻¹; α (initial slope): 6 %. The red and green lines (near the y-axis) show the
1231 modeled elevations of the coral reef terrace (CRT) inner edges, close to or
1232 different from field measurements, respectively.

Supporting information captions – Animation

1233

1234

Supporting Information – S1 - B05 animation

1236

1237 This animation is realised over the past 800 ka with the best-fit numerical
1238 simulation from the sea level reconstruction of Bintanja et al., (2005), i.e., B05,
1239 and with U (uplift rate): 0.50 mm a^{-1} , G_{max} (maximum reef growth rate): 6 mm
1240 a^{-1} , E (erosion rate): $60 \text{ mm}^3 \text{ a}^{-1}$, and α (initial slope): 6 %.

1241

Supporting Information – S2 - W02 animation

1243

1244 This animation is realised over the past 800 ka with the best-fit numerical
1245 simulation from the sea level reconstruction of Waelbroeck et al., (2002), i.e.,
1246 W02, and with U (uplift rate): 0.45 mm a^{-1} , G_{max} (maximum reef growth rate):
1247 6 mm a^{-1} , E (erosion rate): $60 \text{ mm}^3 \text{ a}^{-1}$, and α (initial slope): 6 %. From 800 ka
1248 to 430 ka, the sea level reconstruction of Bintanja et al, (2005) is used, from
1249 430 ka to 0 ka the sea level reconstruction of Waelbroeck et al., (2002).

1250

Supporting Information – S3 - R09 animation

1252

1253 This animation is realised over the past 800 ka with the best-fit numerical
1254 simulation from the sea level reconstruction of Rohling et al., (2009), i.e., R09,
1255 and with U (uplift rate): 0.46 mm a^{-1} , G_{max} (maximum reef growth rate): 6 mm
1256 a^{-1} , E (erosion rate): $60 \text{ mm}^3 \text{ a}^{-1}$, and α (initial slope): 6 %. From 800 ka to 430
1257 ka, the sea level reconstruction of Bintanja et al, (2005) is used, from 500 ka to

1258 0 ka the sea level reconstruction of Rohling et al., (2009).

1259

1260 **Supporting Information – S4 - G14 animation**

1261

1262 This animation is realised over the past 800 ka with the best-fit numerical
1263 simulation from the sea level reconstruction of Grant et al., (2014), i.e., G14,
1264 and with U (uplift rate): 0.50 mm a^{-1} , G_{max} (maximum reef growth rate): 6 mm
1265 a^{-1} , E (erosion rate): $60 \text{ mm}^3 \text{ a}^{-1}$, and α (initial slope): 7 %. From 800 ka to 430
1266 ka, the sea level reconstruction of Bintanja et al, (2005) is used, from 500 ka to
1267 0 ka the sea level reconstruction of Grant et al., (2014).

1268

1269 **Supporting Information – S5 - S16 animation**

1270

1271 This animation is realised over the past 800 ka with the best-fit numerical
1272 simulation from the sea level reconstruction of Spratt and Lisiecki, i.e., S16, and
1273 with U (uplift rate): 0.45 mm a^{-1} , G_{max} (maximum reef growth rate): 6 mm a^{-1} ,
1274 E (erosion rate): $60 \text{ mm}^3 \text{ a}^{-1}$, and α (initial slope): 6 %.